Reponses to reviewer 1
This study investigates the effect of the city of Houston on a convective storm by means of regional numerical simulations. The authors use the WRF model coupled to a bin microphysics scheme and a land surface scheme. The city effect is decomposed into the land effect (the urban heat island effect) and the urban aerosol effect. The aerosol effect is further decomposed into the direct effect (aerosol-radiation interactions, ARI) and the indirect effect (aerosol-cloud interactions, ACI). It is shown that both effects (land and aerosol) drive increase in the convective intensity and precipitation, with the aerosol effect dominate. It is also shown that the interaction between the two effects causes a further intensification of the storm. The aerosol effect is shown to be dominated by the ACI rather than by the ARI. The two effects considered here (land and aerosol) affect the clouds at different stages and different levels in the atmosphere.

We thank the reviewer for your time and constructive comments. We have provided detailed responses point-by-point as below.

The mechanisms behind the different effects are explained. The paper address interesting questions and uses appropriate tools for answering them. I do have a few minor comments and suggestions for the authors:
L26: 15 m/s increase compared to what base-line? Maybe better to present it in percentage change.

The sentence was clear that the increase is the joint effect of both urban land and anthropogenic aerosols therefore it is compared with both effects excluded. The ~15m/s increase is in the maximum updraft speed. Now we have changed to the percentage increase (~75%) (Line 26).

L32: is 40 min change significant? Form the abstract the reader can't evaluate it.

40 min is quite significant since for thunderstorms since the total duration of the case is only a few hours. We have added text about it at Line 494, "…accelerates the development of convective storm into deep cloud stage by ~ 40 min, which is significant for thunderstorms since the storm duration is only a few hours".

L67: It will probably be good to explain what you mean here by: "indirect effect"

Rephrased as "…while aerosols had the opposite effect through the serving as cloud condensation nuclei".

L147: what is the sizes of the domains? From Fig. 1 it looks like domain 2 is of the order of 200-250 km. Is it enough for spin-up of the clouds entering the domain from the lateral boundaries? As the boundary conditions are from MERRA-2 (and not from WRF simulations) I assume that the spin-up requires quite a long time after entering the domain. For a typical windspeed of ~25-30 km/h (Fig. 12, for height below 1 km, and probably even higher windspeed above), the air will spend in the domain about 8- 10 h. Is this enough for the spin-up? In other words, how can you eliminate the domain boundaries effect?

Two nested domains with horizontal grid spacings of 2 and 0.5 km and horizontal grid points of 450 × 350 and 500 × 400 for Domain 1 and Domain 2. The initialization time of Domain 2 is 12-hr ahead of the analysis period for this case, so it is enough for spin-up. The information has been added to the revised manuscript (Line 151 and 169).

L220: are you only integrating liquid and no ice here? As you are simulating deep convective clouds, wouldn't it make more sense to include ice?

Since the tracking algorithm from Hu et al. (2019) used the quantity of vertically integrated liquid (VIL), which is an estimate a vertically-integrated column of radar-retrieved precipitation. VIL was shown to be an effective indicator of strong precipitation cells (Greene and Clark, 1972, Hu et al., 2019). Thus, for the tracking of model results, we used LWP, which an equivalent quantity to VIL) for a fair comparison. We explained this in the previous paragraph by the sentence "To apply the algorithm to both model simulation and NEXRAD observations consistently in this study, we calculated liquid water path (LWP), a variable of model output accounting for the column integrated liquid to replace VIL in MCIT for model simulation". We have also added a sentence to better describe VIL for strong precipitation cells, that is "VIL was shown to be an effective indicator of strong precipitation cells (Greene and Clark, 1972, Hu et al., 2019a)" (Line 225-226).

L233: you have twice "first".

Deleted now.

L381: missing ")"

Added.

L405: what about the role of the slower fall speed of hydrometeors under polluted conditions? As it was shown before, smaller droplets, with lower effective terminal velocity, would be pushed higher into the atmosphere (even for a given vertical velocity) and hence invigorate the ice processes (in addition to the increased latent heating by condensation). Does that play a role here? In addition, in this section it might be a good opportunity to comment on a very relevant recent paper: https://journals.ametsoc.org/doi/pdf/10.1175/JAS-D-20-0012.1

Here we are discussing the enhanced updraft speeds by the anthropogenic aerosol effects. In the updraft cores, updraft speeds are much stronger than the hydrometeor fall speeds so how much droplets are pushed to the high-levels should be determined by updraft speeds. Thus, slower fall speed would not have a large effect. The slower hydrometeor fall speeds do affect stratiform and anvil properties as shown from Fan et al. 2013 (PNAS), Grabowski and Morrison 2016 and 2020 in JAS.
In our case since the increase of latent heating from condensation is much larger than that from the freezing, deposition, and riming (Fig. 15c-d). Therefore, the enhanced vertical velocity is mainly contributed by enhanced condensation. Both Fan et al. (2018) and Lebo (2018) showed that the same amount of latent heating increase at the low-level plays a more significant role in invigorating convection than at the high-levels.

We showed that the higher droplet concentration in the case with anthropogenic aerosols enhances condensation therefore thermal buoyancy since condensation rates depend on droplet number and size based on accurate solution of supersaturation. Grabowski and Morrison (2020) interpreted the convective invigoration at low-levels in a different way. We have added a paragraph to discuss this on Page 20, that is,

"Grabowski and Morrison (2020) interpreted this warm-phase convective invigoration at low-levels by aerosols in a different way. They argued supersaturation (S) in updrafts rapidly, within a few seconds, approaches the quasi-equilibrium supersaturation (S_{eq}). With this quasi-steady assumption ($S \approx S_{eq}$), the condensation rate and buoyancy only depend on updraft velocity, not droplet number and size. Thus they concluded that the lower quasi-equilibrium supersaturation in the polluted case than the pristine case is the reason for enhanced buoyancy and updraft velocity, not the enhanced condensation. The problem is that the quasi-steady approximation is invalidated for updrafts where droplet concentrations are low or droplets are growing and their sizes are changing based on the explicit solution of supersaturation (Korolev and Mazin 2003). The explicit theoretical solution of supersaturation showed that condensation depends on droplet number and size besides updraft speeds (Pinsky et al. 2013). Here in this study the quasi-equilibrium supersaturation in the updrafts is generally 2-3 times higher than the true supersaturation, and the phase relaxation time is generally above 10 s above 3-km altitude in the case without anthropogenic aerosols and about 60 s when droplet number is of 10 cm^{-3} which occurs frequently in the convective cores where autoconversion and rain accretion are strong."

Reponses to reviewer 2
The authors have performed a matrix of simulations to investigate the relative roles of urban heat island and aerosol forcing on the behavior of an observed storm in Houston. They find that both mechanisms lead to increased precipitation for a single cell on their study day. This is a valuable approach and a necessary investigation of multiple forcing mechanisms.

The authors use a single microphysical scheme in a single model, which leads to the ability to directly compare the results in the simulation matrix. The authors show that the simulations with full aerosol and land cover effects are better in some respects than those without. The aerosol effect contributes the most toward bringing the simulations closer to the observations of surface precipitation in these simulations ... and the effect is quite significant as noted on lines 345-6. The aerosol dramatically accelerates the growth of the cloud through the mixed phase zone, consistent with prior studies investigating the aerosol invigoration hypothesis.

We thank the reviewer for your time and constructive comments. We have provided detailed responses point-by-point as below.

More generally, the single model used in this study is one among many state of the art models, and as with any parameterization must build in a set of claims about microphysical processes. The study demonstrates that the aerosol invigoration mechanism *can* be large *if* these claims are correct. I would like to see this latter point emphasized more fully. The authors should review of what may or may not be correct about the microphysical process claims embodied in the model.

The most relevant portions of the study that could use clarification are the additional aerosol process models described on lines 133-134. These are relatively new and probably are driving much of the aerosol effects in this study. What are the likely errors in process rates in these parameterizations? What are the likely errors in thermodynamic characterization? Are they as large as the run-to-run difference the authors observe?

The point is not to relitigate prior work in full, but to the extent the authors can clarify the precision of their forecasts the more value the study has in advancing our shared understanding of how to properly model mixed phase microphysics and how to accurately partition the relative roles of aerosol and thermodynamic influences on convection.
Those are all great questions. We have added a paragraph in Summary and Discussion section to address these questions, that is,
"For simulating aerosol-deep convective cloud interactions, there are a few key modeling requirements as summarized in Fan et al. (2016), such as (1) the prognostic supersaturation is needed for secondary aerosol activation, condensation, and evaporation calculations, (2) hydrometeor size distributions need to be prognostic to physically simulate the responses of microphysical processes to CCN changes, and (3) aerosols need to be prognostic, and fixed aerosol concentrations gave unrealistic cloud properties and qualitatively changed aerosol impacts on convective intensity (Fan et al., 2012). With thee SBM used in this study, all these criteria are satisfied. Furthermore, for (3), we are not only prognosing aerosol numbers but also aerosol composition and size distribution by coupling the SBM with the chemistry and aerosol components. With this coupling, the spatial heterogeneity of aerosols is considered. Also, aerosol

regeneration and wet removal processes can be more physically accounted for compared with the WRF-Chem with two-moment bulk schemes (Gao et al., 2016). The spatial heterogeneity of aerosols was shown to play an important role in simulating a torrential rain event observed over Seoul, Korea (Lee et al., 2018). However, bin schemes also have uncertainties in representing ice-related processes mainly due to our poor understanding of convective microphysics such as ice nucleation and riming processes. In particular, the conversions between different ice categories are also determined by threshold sizes or masses. However, those uncertainties are not expected to qualitatively change the warm-phase invigoration mechanism which occurs via enhanced condensation. In the companion paper Zhang et al. (2020), we carried out a small number of ensemble simulations for the anthropogenic aerosol effects for the same case and the results are consistent with this study, indicating this mechanism is robust with the initial thermodynamic and dynamic perturbations. More sophisticated uncertainty qualifications can be done in future with a larger number of ensembles when computer power becomes more advanced."

Below, I also request clarification of the meteorological setting and terminology used by the authors.

Major concerns
The authors claim SBM_anth in Zhang et al. (2020, preprint) is the same as LandAero in this study, but Figs. 7 and 5, respectively, do not match. Likewise, the associated CFADs of reflectivity do not match, though this may be due to a different analysis box size.

Yes, the analysis area is different between the two studies. Here we are focusing on the convective cell in Houston. Besides, Zhang et al. (2020, preprint) represents the ensemble mean of the three ensemble runs with three different initialization time. However, due to the expensive computational cost, we didn't do ensemble runs for No_Land and No_LandAero. The analysis in this study showed the result of one member for fair comparison between four simulations.

Compared to the observations, the CFAD shows significantly enhanced probabilities of moderate reflectivity at high altitudes (line 241). It also significantly underestimates the prevalence of 40-50 dBZ values at and above the homogeneous freezing level. What is the origin of this overestimate? One interpretation of this is that the SBM is too aggressive in the production of smaller ice crystals that grow into snow at high altitudes, at the expense of graupel. Given the authors' interest in an aerosol invigoration pathway, it seems that matching the ice population in glaciated clouds is more important than matching higher reflectivity values at low altitudes, which can result from many intermediate microphysical steps.

We agree that underestimating reflectivity at high levels is probably due to the model biases in simulating snow (should not have much graupel above 10 km). We have added a sentence discussing it, i.e., "At the upper levels (> 10 km), the model underestimates the large reflectivities (> 35 dBZ), suggesting the model does not get enough snow" (Line 250-252).

As the authors note on line 250, rain rates > 2 mm/hr last about 25% longer in the simulation. This is in common among all simulations, and so would seem to indicate a general over-

production of precipitation duration by the SBM scheme overall. This would be consistent with an overactive snow/ice crystal microphysics scheme instead of a shorter-lived cell tied to faster-precipitating graupel. Why is the standard for "better" maximum reflectivity and areal coverage, but not duration of precipitation?

We did bring up the longer precipitation duration bias with the model. Since all simulations get longer duration than the observation, this model bias is not caused by the effects of aerosol and land surface. It could be related to many things such as problems in meteorological conditions, the interactions of microphysics and dynamics, microphysics parameterizations, the coupling of microphysics with other part of physics (PBL, radiative, ..).

Line 88: while Chen et al. (2011) also use the term "prevailing wind," that term is misleading, especially here in a review of how land-atmosphere interactions *generally* work in Houston. The climatological meaning of prevailing wind (c.f. the AMS Glossary) is the expected value of the wind in a given location over a climatological period. For Houston in the summer, the prevailing wind is onshore, from the southeast (https://mesonet.agron.iastate.edu/sites/windrose.phtml?station=IAH&network=TX_ASOS), and that pattern persists for stations further inland. Chen's study is of an anomalous day that may be representative of bad air quality days in Houston, but it is probably not typical of summer wind patterns or sea breeze interactions in Houston. It seems the authors are concerned in this paragraph with describing the general role of Houston's urban environment in influencing the sea breeze, and so this paragraph should be revised to more accurately reflect Houston's environment.

Thank you for the clarification. We have made changes to the sentences of the paragraph that inappropriately used "prevailing" winds. Now it should be accurate to describe the Houston environment. The revised sentences now read as "The strength and inland propagation of sea breeze circulation can be influenced by land/sea surface temperature contrast, land use/land cover, and the synoptic flow (e.g., Angevine et al., 2006; Bao et al., 2005; Chen et al., 2011). Chen et al. (2011) indicated that the existence of the Houston city favored stagnation because the inland penetration of the sea breeze counteracted the synoptic flow in a case study" (Line 86-90).

Line 112: Neither this study nor Zhang et al. (2020) give a synoptic or mesoscale meteorological overview of this case. Where was the trailing front? How did the meteorology, including the sea breeze, develop during the day in comparison to the expected behavior of the land and sea breeze diurnal cycle in Houston? Rosenfeld et al. (2014) is not listed in the references, and the ACPC website is not a suitable reference for long-term archival purposes.

We have added Fig. 1 and the following discussion to give an overview of the synoptic meteorological conditions of the case, i.e., "As shown in Fig. 1a and Fig. 1c, along a trailing front extended zonally across the southeastern United States, the isolated weak convective clouds formed in the late morning. Deep convective cells over Houston and Galveston bay areas developed in the afternoon with the increased solar heating and strengthened sea breeze circulation (Fig. 1b, d). The sea breeze circulation will be shown in a detail in the result section and it was among the typical summer day sea-breeze conditions (Kocen et al., 2013)." (Line 113-118)

Rosenfeld et al. (2014) has been added now. The ACPC website should be permanent. Also, there is no published paper to cite yet for this intercomparison.

Line 227: What is the "sea breeze wind intensity"? How was the sea breeze perturbation wind identified? This is especially important as the authors discuss Fig. 12 (lines 358 and following), where the sea breeze intensity is said to cause the transition to mixed phase cloud.

As we stated in Line 232-235: "the sea breeze wind intensity at a specific time is calculated by averaging the horizontal wind speeds below 1-km altitude along the black line UO in Fig. 4a."

Minor concerns
Line 64: CG lightning enhancements can also be caused by the presence of tall towers (e.g., Kingfield et al., 10.1002/2017gl073449).

We add this to Line65-67 as: "Kingfield et al. (2017) also found that cloud-to-ground lightning enhancements can also be caused by the presence of tall towers".

Line 157: not using met from domain 1? Not clear to me. Revisit after reading rest of paper. Maybe condense into a chart or truth table. I see the point that all domain 2 sims use same meteorology to control for the fact that different aerosols will affect the meteorology on domain two? But if the meteorology is processing the aerosols, how much is the spatiotemporal distribution of aerosols conditioned by the meteorology?

Since there are two Domain 1 simulations with different aerosol scenarios (anthropogenic emissions on and off), and the simulations accounted for the small-scale urban land and aerosol effects on meteorology already. If Domain 2 uses the meteorological fields from Domain 1, the initial/boundary meteorological conditions for the cases with high aerosol loadings (LandAero and No_Land) would be different from those with the low aerosol loadings (No_Aero and No_LandAero). To use the same meteorological fields to drive all simulations carried out over Domain 2 (including those with and without anthropogenic emissions), also to avoid using the forcing that already accounted for small-scale urban land and aerosol effects, we choose MERRA-2 for the initial and lateral boundary conditions for meteorological fields. We have revised the text in that paragraph to be clearer (Line 163-167). Either way (using Domain 1 or MERRA-2) has pros and cons and we chose the one fitting our purpose the best here.

Line 258: The reduction is not 45% from the larger LandAero value. Perhaps the authors used the wrong denominator? Reading approximate values from the graph to confirm the visual impression,
(6.75-4.8)/6.75 = 0.29
(6.75-4.8)/4.8 = 0.41
The claim is repeated on line 449.

Note we are talking about the enhancement of precipitation by urbanization, which should refer to the case without urbanization, i.e., the denominator should be No_LandAero. The calculation is (6.8-4.7)/4.7=0.45.

Line 327 and Fig. 10: Does this total water content include the vapor phase?
Water vapor is not included. This has been noted in the Figure caption now.

Line 331 and Fig. 10: The line marking the onset of the mixed phase cloud (first appearance of blue above the 0°C level) is marked too late in panel b, and perhaps a bit in panel d, making the duration of mixed phase growth artificially short.

The 0°C level is just an approximate mark there. If there is no continuous growing to deeper clouds after the water is a little above the 0°C level, it would still be shallow clouds.

Line 393-4: the phrasing here makes for a confusing physical explanation; "the condensate loading effect is small as a result of enhanced condensational heating" but the condensational heating is directly related to the mass condensed, which should result in more condensate loading.

Sorry the order of the phrases in the original sentence was wrong. It has been revised as "…which is mainly because of the increased thermal buoyancy as a result of enhanced condensational heating since the offset effect of condensate loading is small (Fig. 16a) (Fig. 16c, blue lines)".

1 **Urbanization-induced land and aerosol impacts on sea breeze circulation and convective**

2 **precipitation**

4 Jiwen Fan[1, *], Yuwei Zhang[1, *], Zhanqing Li[2], Jiaxi Hu[3], and Daniel Rosenfeld[4]

6 [1] Atmospheric Sciences and Global Change Division, Pacific Northwest National Laboratory,

7 Richland, WA, USA

8 [2] Department of Atmospheric and Oceanic Science, University of Maryland, College Park, MD,

9 USA

10 [3] University of Oklahoma, and NOAA/OAR National Severe Storms Laboratory, Cooperative

11 Institute for Mesoscale Meteorological Studies, Norman, OK, USA

12 [4] Institute of Earth Sciences, The Hebrew University of Jerusalem, Jerusalem, Israel

13 *Corresponding author:* Jiwen Fan (Jiwen.Fan@pnnl.gov) and Yuwei Zhang
14 (Yuwei.Zhang@pnnl.gov)

Abstract

Changes in land cover and aerosols resulting from urbanization may impact convective clouds and precipitation. Here we investigate how Houston urbanization can modify sea-breeze induced convective cloud and precipitation through urban land effect and anthropogenic aerosol effect. The simulations are carried out with the Chemistry version of the Weather Research and Forecasting model (WRF-Chem), which is coupled with the spectral-bin microphysics (SBM) and the multilayer urban model with a building energy model (BEM-BEP). We find that Houston urbanization (the joint effect of both urban land and anthropogenic aerosols) notably enhances storm intensity (by ~75% in maximum vertical velocity) and precipitation intensity (up to 45%), with the anthropogenic aerosol effect more significant than the urban land effect. Urban land effect modifies convective evolution: speed up the transition from the warm cloud to mixed-phase cloud thus initiating surface rain earlier but slowing down the convective cell dissipation, all of which result from urban heating induced stronger sea breeze circulation. The anthropogenic aerosol effect becomes evident after the cloud evolves into the mixed-phase cloud, accelerating the development of storm from the mixed-phase cloud to deep cloud by ~ 40 min. Through aerosol-cloud interaction (ACI), aerosols boost convective intensity and precipitation mainly by activating numerous ultrafine particles at the mixed-phase and deep cloud stages. This work shows the importance of considering both urban land and anthropogenic aerosol effects for understanding urbanization effects on convective clouds and precipitation.

1 Introduction

Urbanization has been a significant change in the earth's environment since industrialization and is expected to further expand during the coming decades (Agli et al., 2004). Many modeling and observational studies have shown that urbanization can impact weather and climate (e.g., Shepherd et al., 2010; Ashley et al., 2012).

Urbanization could impact storm properties through two major pathways. The first major pathway is through the changes in land cover types. For urban land, the most typical and extensively studied effect is the increase of surface temperature compared to the surrounding rural area, known as the urban heat island (UHI) effect (e.g., Bornstein and Lin, 2000; Shepherd, 2005; Hubbart et al., 2014). Convective storms may be initiated at the UHI convergence zone, created through a combination of increased temperature and mechanical turbulence resulting from complex urban surface geometry and roughness (Bornstein and Lin, 2000; Shepherd, 2005, Hubbart et al., 2014). Urban landscapes impact sensible and latent heat flux, soil moisture, etc., affecting thunderstorm initiation (Haberlie et al., 2015) and changing the location and amount of precipitation compared to the pre-urbanization period (Shepherd et al. 2002; Niyogi et al. 2011).

The second major pathway of the urbanization impacts is through pollutant aerosols associated with industrial and population growth in cities. Previous studies have shown that urban aerosols invigorate precipitation in urban downwind regions through aerosol-cloud interaction (ACI; Van den Heever and Cotton 2007; Carrió et al. 2010; Fan et al., 2018). A recent study showed aerosol spatial variability in the Seoul area played an important role in a torrential rain event (Lee et al., 2018). Many compelling pieces of evidence have emerged showing the joint influences of aerosols and urban land on clouds and precipitation, especially in China where both effects are strong and complex (Li et al., 2019 and references therein).

61   The majority of the past studies focused on one of the abovementioned pathways.

62   Recently, a few studies examined the combined effects of both pathways on lightning and

63   precipitation. A new observational study (Kar and Liou, 2019) indicated that both land and

64   aerosol effects should be considered to explain the cloud-to-ground lightning enhancements over

65   the urban areas. Kingfield et al (2017) also found that cloud-to-ground lightning enhancements

66   can also be caused by the presence of tall towers. A modeling study showed urban land-cover

67   changes increased precipitation over the upstream region but decreased precipitation over the

68   downstream region, while aerosols had the opposite effect through serving as cloud condensation

69   nuclei (Zhong et al. 2015). A long-period (5 years) modeling study in the Yangtze River Delta

70   (YRD) region confirmed the opposite effects on precipitation but the aerosol radiative effect was

71   the dominant reason for the reduced convective intensity and precipitation (Zhong et al. 2017).

72   Sarangi et al. (2018) also showed the enhanced precipitation over the urban core by the urban

73   land effect and at the downwind region by the aerosol effect, consistent with Zhong et al (2015).

74   Schmid and Niyogi (2017) showed that urban precipitation rate enhancement is due to a

75   combination of land heterogeneity induced dynamical lifting effect and aerosol indirect effects.

76   For coastal cities, studies indicated that anthropogenic aerosol effect on precipitation may be

77   more important than the urban land effect (Liu and Niyogi et al., 2019, Ganeshan et al., 2013;

78   Ochoa et al., 2015).

79   Houston is the largest city in the southern United States. It is one of the most polluted

80   areas in the nation based on the most recent "State of the Air" report by the American Lung

81   Association (http://www.stateoftheair.org/about/). The Houston urbanization causes both land

82   cover change and anthropogenic emission enhancement which has been a fertile region for air

83   quality studies (i.e., high ozone) (e.g., Chen et al., 2011, Fast et al., 2006). The sea breeze

84   circulation over the region plays a key role not only in convection and precipitation but also in

85   local air quality (Fan et al., 2007; Banta et al. 2005, Caicedo et al., 2019). The strength and

86   inland propagation of sea breeze circulation can be influenced by land/sea surface temperature

87   contrast, land use/land cover, and the synoptic flow (e.g., Angevine et al., 2006; Bao et al., 2005;

88   Chen et al., 2011). Chen et al. (2011) indicated that the existence of the Houston city favored

89   stagnation because the inland penetration of the sea breeze counteracted the synoptic flow in a

90   case study. On the other hand, Ryu et al. (2016) showed the urban heating of the Baltimore–

91   Washington metropolitan area strengthened the bay breeze thus promoted intense convection and

92   heavy rainfall. In Shanghai, however, the sea-land breeze has exhibited a weakening trend over

93   the past 21 years, which was hypothesized to result from the joint influences of aerosol, UHI,

94   and greenhouse effects (Shen et al., 2019). While sorting out the various factors is a daunting

95   task especially by means of observation analysis, it is essential to enhance our understanding of

96   both overall effects by human activity and individual ones for which much fewer have been

97   done.

98   In this study, we aim at understanding how the changes in Houston land cover and

99   anthropogenic aerosols as a result of urbanization modify the sea-breeze induced convective

100   storm and precipitation jointly and respectively. To answer the science question, we employ the

101   Chemistry version of Weather Research and Forecast (WRF) model coupled with the spectral-

102   bin microphysics (WRF-Chem-SBM) scheme, a model we previously developed and applied to

103   warm stratocumulus clouds (Gao et al., 2016), to simulate a deep convective storm case that

104   occurred over the Houston region and produced heavy precipitation. Sensitivity tests are

105   performed to look into the joint and respective effects of urban land and anthropogenic aerosol

106   on storm development and precipitation.

2 Case Description, Model, and Analysis Method

2.1 Case description

The deep convective cloud event we simulate in this study occurred on 19-20 June 2013 near Houston, Texas. The case was also selected for the ACPC Model Intercomparison Project (Rosenfeld et al., 2014; www.acpcinitiative.org). In another companion study (Zhang et al., 2020), this case was simulated to study the impact of cloud microphysics parameterizations on ACI. As shown in Fig. 1a and Fig. 1c, along a trailing front extended zonally across the southeastern United States, the isolated weak convective clouds formed in the late morning. Deep convective cells over Houston and Galveston bay areas developed in the afternoon with the increased solar heating and strengthened sea breeze circulation (Fig. 1b, d). The sea breeze circulation will be shown in a detail in the result section and it was among the typical summer day sea-breeze conditions (Kocen et al., 2013). A strong convective cell observed in the Houston city that we focused on was initiated at 2145 UTC (local time 16:45) and developed to its peak precipitation at 2217 UTC.

The simulated case was evaluated extensively in aerosol and cloud properties in the companion paper mentioned above. The observations of radar reflectivity and precipitation are also used in the evaluation. The radar reflectivity is obtained from the Next-Generation Weather Radar (NEXRAD) network for the KHGX site at https://www.ncdc.noaa.gov/data-access/radar-data/nexrad-products, with a temporal frequency of every ~5 minutes and a spatial resolution of 1 km. The high-temporal and spatial precipitation data retrieved based on radar reflectivity is used for simulation evaluation.

2.2 Model description and experiment design

The WRF-Chem-SBM model used in this study is based on Gao et al. (2016), with updates in both WRF-Chem (Grell et al., 2005; Skamarock et al., 2008) and the SBM (Khain et al., 2004; Fan et al., 2012). The SBM version coupled with WRF-Chem is a fast version with only four sets of 33 bins for representing size distribution of CCN, drop, ice/snow, and graupel/hail, respectively. It is currently coupled with the four-sector version of the Model for Simulating Aerosol Interactions and Chemistry (MOSAIC) (Fast et al., 2006; Zaveri et al., 2008). Compared with the original WRF-Chem model which uses two-moment bulk microphysics schemes, besides the advancements in cloud microphysical process calculations in SBM, the aerosol-cloud interaction processes which impact both cloud and aerosol properties are physically improved. These processes are aerosol activation, resuspension, and in-cloud wet-removal (Gao et al., 2016). Theoretically, both aerosol and cloud processes can be more realistically simulated compared with the original WRF-Chem, particularly under the conditions of complicated aerosol compositions and aerosol spatial heterogeneity. This would result in improved simulations of both ACI and aerosol-radiation interactions (ARI). Following on Gao et al. (2016) where the model was applied to a warm stratocumulus cloud case, we apply the model to the deep convective storm case in this study.

The dynamic core of WRF-Chem-SBM is the Advanced Research WRF model that is fully compressible and non-hydrostatic with a terrain-following hydrostatic pressure vertical coordinate (Skamarock et al., 2008). The grid staggering is the Arakawa C-grid. The model uses the Runge-Kutta 3rd order time integration schemes, and the 3rd and 5th order advection schemes are selected for the vertical and horizontal directions, respectively. The positive-definite option is employed for the advection of moist and scalar variables.

150   The model domains are shown in Fig. 2. Two nested domains have horizontal grid

151   spacings of 2 and 0.5 km and horizontal grid points of 450×350 and 500×400, respectively,

152   with 51 vertical levels up to 50 hPa. Domain 1 simulations are run with WRF-Chem using

153   Morrison double-moment scheme (Morrison et al., 2005) to produce realistic aerosol fields for

154   Domain 2 simulations. Two simulations were run over Domain 1 with anthropogenic emissions

155   turned on and off, respectively, starting from 0000 UTC 14 Jun and ending at 1200 UTC 20 June

156   with about 5 days for chemical spin up. The chemical lateral boundary and initial conditions for

157   Domain 1 simulations were from a quasi-global WRF-Chem simulation at 1-degree grid spacing,

158   and meteorological lateral boundary and initial conditions were created from MERRA-2 (Gelaro

159   et al., 2017). Domain 2 simulations use WRF-Chem-SBM, driven with the initial and lateral

160   boundary aerosol and chemical fields from Domain 1 outputs, but the initial and lateral boundary

161   conditions for meteorological fields are from MERRA-2. The reason for not using the

162   meteorological fields from Domain 1 simulations is that the meteorological fields are different

163   between the two Domain 1 simulations with and without anthropogenic emissions. To use the

164   same meteorological fields to drive all simulations carried out over Domain 2 (including those

165   with and without anthropogenic emissions), also to avoid using the forcing that already

166   accounted for small-scale urban land and aerosol effects, we choose MERRA-2 for the initial and

167   lateral boundary conditions for meteorological fields. Domain 2 simulations are initiated at 0600

168   UTC 19 June (~ 5 days later from the initial time of Domain 1 simulations) and run for 30 hours.

169   The analysis period is ~ 12 hours after the initiation time of Domain 2. The modeled dynamic

170   time step was 6 s for Domain 1 simulations and 3 s for Domain 2 simulations.

171   For all simulations over both domains, the anthropogenic emission was from NEI-2011

172   emissions. The biogenic emission came from the Model of Emissions of Gases and Aerosols

173   from Nature (MEGAN) product (Guenther et al., 2006). The biomass burning emission was from

174   the Fire Inventory from NCAR (FINN) model (Wiedinmyer et al., 2011).

175   The baseline simulation over Domain 2 uses the initial and boundary chemical and

176   aerosol conditions from the Domain 1 simulation with anthropogenic emissions turned on. This

177   simulation uses all available emissions as abovementioned including anthropogenic emissions. It

178   is the same simulation as "SBM_anth" in Zhang et al. (2020). Here we renamed it "LandAero",

179   in which the effects of urban land and anthropogenic aerosols are considered (Fig. 3a, c). Based

180   on LandAero, sensitivity tests are conducted to investigate the combined and individual effects

181   of urban land and anthropogenic aerosols. No_Aero is the simulation based on LandAero, except

182   that anthropogenic emissions are turned off and the initial and boundary chemical and aerosol

183   conditions are from the Domain 1 simulation without anthropogenic aerosols considered (Fig.

184   3b). No_Land is also based on LandAero, except the Houston urban land is replaced by the

185   surrounding cropland and pasture (Fig. 3d). The aerosols used in No_Land include the

186   anthropogenic sources (Fig. 3a), which is analogous to the scenario of downwind a big city (i.e.,

187   rural area with pollution particles transported from the city). We also run a simulation with both

188   the urban land cover replaced by the surrounding cropland and the anthropogenic aerosols

189   excluded (Fig. 3b, d), which is referred to as "No_LandAero". That is, both effects of urban land

190   and anthropogenic aerosol are not considered in this simulation. By comparing LandAero with

191   No_LandAero, the joint effect of urban land and anthropogenic aerosols can be obtained. The

192   individual urban land and anthropogenic aerosol effect can be obtained by comparing LandAero

193   with No_Land and LandAero with No_Aero, respectively.

194   The simulated aerosol and CCN properties are evaluated with observations in Zhang et al.

195   (2020), which shows that the model captures aerosol mass and CCN number concentrations

196   reasonably well. Aerosol number concentration is not evaluated because the measurements are

197   not available at the Texas Commission for Environmental Quality (TCEQ) sites. A snapshot of

198   simulated aerosol number concentrations in LandAero and No_Aero at the time of 6 hours before

199   the initiation of the Houston cell is shown in Fig. 3a-b. Houston anthropogenic emissions

200   produce about 10 times more aerosol concentrations over the Houston area than those in the Gulf

201   of Mexico and ~ 5 times than those in the rural area shown in Fig. 3a. The background aerosol

202   concentrations are relatively low (around 250 cm^{-3}) in this region. Aerosols over the Houston

203   urban area are mainly contributed by organic aerosols, which are highly related to the oil refinery

204   industry and ship channel emissions. The aerosol compositions are mainly sulfate in the rural

205   area and sea salt over the Gulf of Mexico in our simulations. Therefore, aerosol properties are

206   extremely heterogenous in this region. Fig. 4 shows the mean aerosol size distributions from the

207   three areas as marked up in Fig. 3a in LandAero. In the Houston area, the majority of aerosols

208   (75%) have a size (diameter) smaller than 100 nm, and 51% of the aerosols are ultrafine aerosol

209   particles (smaller than 60 nm). Those small particles are substantially reduced in the rural area

210   and the Gulf of Mexico (Fig. 4).

211   To see how the land cover type change affects temperature, Fig. 5 shows the differences

212   in 2-m temperature and surface sensible heat fluxes between LandAero and No_Land at 1600

213   UTC when the sea breeze begins to show differences. The urban land increases near-surface

214   temperature over Houston and its downwind area by about 1-2 °C (Fig. 5a), corresponding to the

215   increase of surface sensible heat fluxes (Fig. 5b). More information about the temporal evolution

216   and vertical distribution of the urban heating will be discussed in the result section.

2.3 Analysis Method

217

218   To quantify the convective cell properties occurring over Houston, we employ the Multi-

219   Cell Identification and Tracking (MCIT) Algorithm from Hu et al. (2019a) to track the

220   convective storms. The MCIT is a watershed-based algorithm and shows better tracking

221   capabilities compared with traditional centroid based tracking algorithms. The MCIT identifies

222   cells by local maxima of vertically integrated liquid (VIL) based on watershed principles and

223   performs tracking of multiple cells based on maximum common VIL between the consecutive

224   scans. In this way, convective storm life cycle from initiation to dissipation can be better tracked

225   than the traditional methods as detailed in Hu et al. (2019a). VIL was shown to be an effective

226   indicator of strong precipitation cells (Greene and Clark, 1972, Hu et al., 2019a).

227   To apply the algorithm to both model simulation and NEXRAD observations

228   consistently in this study, we calculated liquid water path (LWP), a variable of model output

229   accounting for the column integrated liquid to replace VIL in MCIT for model simulation. We

230   track local maxima of LWP by identifying the two cells in consecutive radar scans that have

231   maximum common LWP. A cell is identified and tracked when the local maxima LWP exceeds

232   50 g m^{-2}. This value is selected because it allows us to start recognizing the deep convective cell

233   by filtering a lot of shallow clouds surrounded it. The storm area of the tracked cell is defined as

234   the grid area with LWP > 50 g m^{-2}.

235   To examine sea breeze circulation over the Houston region, the sea breeze wind intensity

236   at a specific time is calculated by averaging the horizontal wind speeds below 1-km altitude

237   along the black line UO in Fig. 5a. The cross section of the winds along this line is also analyzed

238   in the result section.

3 Results

3.1 Radar reflectivity, precipitation, and convective intensity

We first discuss the evaluation of the baseline simulation LandAero. The simulation is comprehensively evaluated in Zhang et al. (2020). Here the comparisons with observed radar reflectivity and precipitation are included. The composite radar reflectivity at the time of the peak reflectivity of the storm in Houston shows that LandAero captures the convective cell in Houston, with the maximal radar reflectivity of 58 dBZ, very close to the observed 57 dBZ (Fig. 6a, b). The modeled convective cell in LandAero has a larger size compared with the radar observations. The contoured frequency by altitude diagram (CFAD) over the major storm period (1800 UTC 19 Jun to 0000 UTC 20 Jun) shows that the model overestimates the frequencies of moderate reflectivity (i.e., 15-35 dBZ) over the entire vertical profile (Fig. 7a-b), but captures the occurrence frequencies of high reflectivity (larger than 45 dBZ) reasonably well. At the upper levels (> 10 km), the model underestimates the large reflectivities (> 35 dBZ), suggesting the model does not get enough snow. The magnitude of the surface rain rate averaged over the study area defined by the red box in Fig. 6 from LandAero agrees with the retrieved value from the NEXRAD reflectivity, with a peak time about 40 min earlier than the observation (Fig. 8a). The probability density function (PDF) of rain rates shows that LandAero reproduces the occurrence frequencies of low and mediate rain rates well (left two columns in Fig. 8b) and overestimates the occurrence frequencies of high rain rates (> 10 mm h^{-1}; right two columns in Fig. 8b). The accumulated precipitation over the time period shown in Fig. 8a is about 7.2 mm from LandAero and 5.5 mm from observations, with a model overestimated of ~ 30% because of the overestimation of occurrences of high rain rates and a longer precipitation period.

261   Without Houston urbanization (i.e., both effects of urban land and anthropogenic aerosol

262   are removed), the Houston convective cell is a lot smaller in the area and has reflectivity values

263   of ~ 7 dBZ lower in general compared with LandAero and the NEXRAD observation (Fig. 6c vs.

264   5a-b). There is almost no radar reflectivity larger than 50 dBZ in No_LandAero (Fig. 7c), in

265   contrast with the significant occurrences of reflectivity larger than 50 dBZ in LandAero and the

266   NEXRAD observation. Those differences are more clearly shown in Fig. 7f. The peak surface

267   rain rate in No_LandAero is reduced by ~ 45% compared with LandAero and observations (Fig.

268   8a; black vs. red line), with the occurrences of large rain rates (> 15 mm h^{-1}) reduced by nearly

269   an order of magnitude (Fig. 8b). In terms of updraft intensity, the CFAD plots in Fig. 9a-b show

270   that there is extremely low or no occurrence for updraft velocity larger than 15 m s^{-1} in

271   No_LandAero, while the occurrences of 30 m s^{-1} still exist in LandAero. There are fewer

272   occurrences of weak updraft velocities and more occurrences of relatively strong updraft

273   velocities over the vertical profile (Fig. 9e). These results indicate the urbanization (i.e., the joint

274   urban land and aerosol effects) drastically enhances the convective intensity and precipitation.

275   Now let's look at the individual effect from the Houston urban land and anthropogenic

276   aerosols. Fig. 6 shows that the urban land effect enlarges the storm area (Fig. 6d vs. 5b) but the

277   aerosol effect is more significant (Fig. 6e vs. 5b). The CFAD of radar reflectivity in Fig. 7 also

278   shows that changes in the PDF by the urban land effect is notably smaller than the anthropogenic

279   aerosol effect. For the occurrence frequencies of high reflectivity larger than 48 dBZ, the change

280   is mainly from the anthropogenic aerosol effect (Fig. 7f-h).

281   For precipitation, we do not see an important effect of urban land on the magnitudes of

282   precipitation rate and the PDF of rain rate (Fig. 8a-b; No_Land vs LandAero). The accumulated

283   rain is about 6.9 mm, which is also not much different from 7.2 mm in LandAero. On the

284 contrary, the anthropogenic aerosol effect increases the peak rate by ~ 30%. The frequency of

285 large rain rates (> 15 mm h^{-1}) is increased by about 5 times (Fig. 8b; No_Aero vs LandAero).

286 The joint effect of both urban land and aerosol increases the accumulated rain by ~ 26%, the

287 peak rain rates by 45%, and the frequency of large rain rates by an order of magnitudes (from

288 No_LandAero to LandAero), suggesting the interactions between the two factors amplify the

289 effect on precipitation, particularly on the large rain rates. Although the Houston urban land

290 alone does not much affect the magnitude of precipitation, the initial time of the rain is advanced

291 by ~ 30 min from No_Land to LandAero (Fig. 8a), indicating that the urban land effect speeds

292 up the rain formation. Aerosol effect delays the initial and peaks rain by ~ 10 min (from

293 No_Aero to LandAero). This will be further discussed in Section 3.2 on convective evolution.

294   On convective intensity, the large increases in occurrence frequencies of the updraft

295 speed greater than 10 m s^{-1} in the upper-levels by the joint effect are mainly contributed by the

296 anthropogenic aerosol effect (Fig. 9e, g). Below 6 km, both the urban land and aerosol effects

297 play evident roles in increasing the occurrences of relatively large updraft speeds (Fig. 9e-g). The

298 larger anthropogenic aerosol effect is also clearly seen from the occurrences of maximal vertical

299 velocity: ~ 30 m s^{-1} in LandAero, while only ~19 m s^{-1} in No_Aero when the anthropogenic

300 aerosol effect is removed, whereas the value is 27 m s^{-1} in No_Land when the urban land effect

301 is turned off (Fig. 9a, c-d). The large effect of anthropogenic aerosols on convective intensity

302 supports the significant aerosol effects on large precipitation rates as shown in Fig. 8. With both

303 effects removed (No_LandAero), there is almost a 100% reduction for the vertical velocity

304 greater than ~ 15 m s^{-1}, showing a quite strong enhancement of convective intensity as a result of

305 urbanization, mainly through the anthropogenic aerosol effects.

3.2 Convective evolution

The urban land effect initiates surface rain about 30 minutes earlier as discussed above, suggesting that convective cloud development is affected when the urban land effect is considered. We examine the convective evolution for the cell over Houston using the cell-tracking method described in Section 2. The time evolution of the tracked cell properties is shown in Fig. 10a-b. Clearly, the urban land effect enhances the reflectivity and area for the tracked cell over the lifetime (from the black dashed line to black solid line), and it also accelerates the development to the peak reflectivity but slows down the dissipation after the peak radar reflectivity is reached (Fig. 10a-b). The anthropogenic aerosols also enhance the convective cell reflectivity and area throughout the cell lifecycle (from the black dotted line to black solid line), with a much larger effect compared with the urban land effect. The anthropogenic aerosol effect does not affect the timing of peak reflectivity (dotted vs. solid black in Fig. 10a-b). The overall reflectivity and cell area properties are shown in Fig. 10c-d, which presents a consistent story as Fig. 10a-b. The baseline simulation LandAero tends to overestimate the frequency of big cell sizes (200-300 km^2) and underpredict the frequency of small cell size (Fig. 10d). Since LandAero predicts a similar rain intensity and rain rate PDF as observations as discussed above, this means that a larger storm cell than observations is needed to predict a similar precipitation intensity as observations. For this reason, No_LandAero which predicts much smaller cell size agrees better with the observations compared with the other simulations purely based on cell size (Fig. 10b, d). However, as discussed above, other metrics such as peak precipitation rate and PDF do not support it. It also should be noted that radar reflectivity in model calculation has a large uncertainty and the model's overestimation can be partly the result of crude Rayleigh scattering assumptions applied to the model fields. The model overestimation of radar

329 reflectivity has been commonly found in previous studies at cloud-resolving scales (Varble et al.

330 2011; 2014, Fan et al., 2015; 2017).

331   Since the small and numerous shallow cumulus clouds are difficult to be tracked with cell

332 tracking algorithm and they are excluded from the above tracking, to examine how the

333 convective storm evolves from the initial shallow cumulus period, we chose the red box shown

334 in Fig. 6 which contains the Houston cell as the study area. Since the convective storm does not

335 spatially move much with time in this study, this is a valid way to look at the temporal evolution.

336 Fig. 11 shows the temporal evolution of the maximal total water content (TWC; color contours)

337 at each level and the maximal vertical velocity in the study area (black line). The convective

338 storm has three distinct periods: warm cloud, mixed-phase cloud, and deep cloud. The mixed-

339 phase and deep cloud are defined with a cloud top temperature (cloud top is defined with TWC >

340 0.01 g kg^{-1} at the topmost level) between 0 and -40 ⁰C and below -40 ⁰C, respectively. The purple

341 and black dashed lines in Fig. 11 mark the initiation of mixed-phase and deep clouds,

342 respectively.

343   As we can see, there is a relatively long warm cloud period for this case (Fig. 11a). With

344 both urban land and anthropogenic aerosol effects removed, the cloud development from the

345 warm cloud to mixed-phase cloud is delayed by ~ 30 min (Fig. 11d vs. 10a), so is the

346 development from the mixed-phase cloud to deep cloud. Compared Fig. 11a with 10b and 10c,

347 we see that it is mainly the urban land effect that enhances the development of warm cloud to the

348 mixed-phase cloud by nearly 30 min, while aerosol effect does not affect it (Fig. 11a vs. 10c).

349 However, it is mainly the aerosol effect that accelerates the development from the mixed-phase

350 cloud to deep cloud by about 35 min. In the case of the urban land effect removed (i.e.,

351 No_Land; Fig. 11b), the anthropogenic aerosol effect makes the duration of the mixed-phase

352   cloud very short - about 35 mins shorter relative to LandAero in which both effects are

353   considered and 75 min shorter relative to No_Aero in which aerosol effect is removed but the

354   urban land effect is considered. This is due to the aerosol invigoration effect in the mixed-phase

355   cloud stage which will be elaborated later.

356   Accompanying with the faster development of warm cloud to mixed-phase cloud by the

357   urban land effect is the stronger updraft speeds in the warm cloud stage (shown from the

358   maximal updraft velocity in Fig. 11 and the mean of the top 25th percentile updraft speeds in Fig.

359   12a). Similarly, for the simulations with the aerosol effect considered (i.e., LandAero and

360   No_Land), the convection is stronger in the mixed-phase cloud stage (Fig. 12b), which

361   accelerates the development into the deep cloud.

362   Now the questions are: (1) how does the urban land effect enhance convective intensity at

363   the warm cloud stage and speeds up the cloud development from the warm to mixed-phase

364   cloud, but slows down the storm dissipation? (2) how do the anthropogenic aerosols increase

365   convective intensity at the mixed-phase cloud stage and accelerate the development of mixed-

366   phase into the deep cloud?

367   For Question (1), Fig. 11a and Fig. 13a show that the development of the warm cloud to

368   mixed-phase cloud occurs when the sea breeze circulation reaches its strongest. Also, the

369   development corresponds to the fastest and largest increase of sea breeze intensity by the urban

370   land effect (Fig. 13a). Anthropogenic aerosol does not seem to affect sea breeze circulation. The

371   enhanced sea breeze circulation in the simulations with the urban land effect considered (i.e.,

372   LandAero and No_Aero) compared with No_Land and No_LandAero corresponds to the

373   increases of surface sensible heat flux and air temperature at low levels (Fig. 13b, d), which is

374   so-called "urban heat island". The urban heating effect on temperature is significant up to 0.8-km

375   altitude at its strongest time that also corresponds to the strongest sea breeze time (Fig. 14b). The

376   urban heating enhances convergence in Houston and at the same time increases the temperature

377   differences between Houston and the Gulf of Mexico, both of which would contribute to a

378   stronger sea breeze circulation. Past studies showed that urban roughness could also enhance

379   low-level convergence (e.g., Niyogi et al., 2006). However, the majority of the studies indicated

380   that increased surface sensible heat flux is the main reason for the enhanced convergence (Liu

381   and Niyogi, 2019; Shimadera et al., 2015).

382   The stronger sea breeze circulation transports more water vapor to Houston (Fig. 15). At

383   the time 1930 UTC when the sea breeze is strongest and the enhancement is the largest (Fig.

384   13a), as well as the temperature contrast between the Houston urban area and the Gulf of Mexico

385   is the largest (Fig. 14b), the low-level moisture in the urban area is clearly higher in LandAero

386   compared with No_Land (Fig. 15b, color contour), which would help enhance convection. As a

387   result, the updraft speed of the Houston convective cell is much larger in LandAero compared

388   with No_Land (Fig. 15b, contoured line). The stronger convection continues even when sea

389   breeze dissipates (Fig. 15c) because the heating effect in the urban area extends to the nighttime

390   until 2300 UTC (local time 18:00; Fig. 13c-d and 13c). This explains the slower dissipation of

391   the tracked Houston cell by the urban land effect as shown in Fig. 10a-b. In a word, the urban

392   heating along with the strengthened sea breeze circulation induced by the urban heating enhances

393   convection at the warm cloud stage and speeds up the development from the warm to mixed-

394   phase cloud, and the temporally-extended urban heating effect leads to a slower dissipation of

395   the convective cell.

396   For Question (2), which is about how anthropogenic aerosols increase convective intensity

397   at the mixed-phase cloud stage and accelerate the development of mixed-phase into deep cloud,

398   Fig. 12b shows the anthropogenic aerosol effect on updraft speeds becomes notable at the mixed-

399   phase cloud stage, the effect is doubled compared with the urban land effect at the mixed-phase

400   regime (6-9 km altitudes). This corresponds to the increased net buoyancy (Fig. 16a, black lines)

401   at those levels from No_Aero to LandAero, which is mainly because of the increased thermal

402   buoyancy as a result of enhanced condensational heating since the offset effect of condensate

403   loading is small (Fig. 16a) (Fig. 16c, blue lines). The condensational heating increase is most

404   significant at 3-5 km and 6-9 km altitudes, corresponding to notably increased secondary droplet

405   nucleation of small aerosol particles which are not able to be activated at the cloud base (Fig. 16e).

406   In this case, aerosols with a diameter smaller than 80 nm but larger than 39 nm (the smallest size

407   in the 4-sectional MOSAIC), which account for about two-thirds of the total simulated aerosols,

408   are not activated around cloud bases. All of them can be activated in the strong updrafts (Fan et

409   al., 2018). This strong secondary nucleation leads to increased droplet number and mass by the

410   anthropogenic aerosol effects (from No_Aero to LandAero; Fig. 17a, c). To recap, the

411   anthropogenic aerosols enhance updraft velocity at the mixed-phase cloud stage mainly through

412   enhanced condensation heating (i.e., "warm-phase invigoration"), as a result of nucleating small

413   aerosol particles below 60 nm which are transported to higher-levels. Enhanced secondary

414   nucleation promotes condensation because of larger integrated droplet surface area associated with

415   a higher number of small droplets (Fan et al., 2007, 2013. 2018; Khain et al., 2012; Sheffield et

416   al., 2015; Lebo, 2018). Thus, the stronger convection speeds up the development of mixed-phase

417   into deep cloud from No_Aero to LandAero. For the same reason, a similar acceleration is seen in

418   No_Land compared with No_Aero and No_LandAero because the anthropogenic aerosol effect is

419   considered in No_Land.

420   Grabowski and Morrison (2020) interpreted this warm-phase convective invigoration at

421   low-levels by aerosols in a different way. They argued supersaturation (S) in updrafts rapidly,

422   within a few seconds, approaches the quasi-equilibrium supersaturation (S_{eq}). With this quasi-

423   steady assumption ($S \approx S_{eq}$), the condensation rate and buoyancy only depend on updraft velocity,

424   not droplet number and size. Thus they concluded that the lower quasi-equilibrium supersaturation

425   in the polluted case than the pristine case is the reason for enhanced buoyancy and updraft velocity,

426   not the enhanced condensation. The problem is that the quasi-steady approximation is invalidated

427   for updrafts where droplet concentrations are low or droplets are growing and their sizes are

428   changing based on the explicit solution of supersaturation (Korolev and Mazin 2003). The explicit

429   theoretical solution of supersaturation showed that condensation depends on droplet number and

430   size besides updraft speeds (Pinsky et al. 2013). Here in this study the quasi-equilibrium

431   supersaturation in the updrafts is generally 2-3 times higher than the true supersaturation, and the

432   phase relaxation time is generally above 10 s above 3-km altitude in the case without

433   anthropogenic aerosols and about 60 s when droplet number is of 10 cm^{-3} which occurs frequently

434   in the convective cores where autoconversion and rain accretion are strong.

435   At the deep cloud stage, the anthropogenic aerosol effect becomes more significant

436   compared with that in the mixed-phase cloud stage (Fig. 12c vs. 11b), particularly at the low-

437   levels. We can still see the enhancement of convective intensity by the urban land effect

438   although the sea breeze difference is relatively smaller at this stage as explained above. The

439   larger aerosol effect at the deep cloud stage compared with the mixed-phase cloud stage is

440   because the secondary droplet nucleation above the cloud base becomes larger (Fig. 16f). More

441   aerosols get activated is the result of higher supersaturation since (a) updrafts are stronger than

442   the mixed-phase cloud stage and (b) more rain forms and removes droplet surface area for

443   condensation (Fan et. al., 2018). As a result, the latent heating from condensation and then the

444   thermal buoyancy is increased in a larger magnitude (Fig. 16b, d), thus a larger aerosol impact is

445   seen at the deep cloud stage. The invigorated deep convection has up to 2 times more ice particle

446   number concentration and 30% larger ice particle mass mixing ratio (Fig. 17b, d), with the

447   maximal cloud top height increased by ~ 1 km. The enhanced ice number and mass

448   concentrations also partially result from the freezing of more droplets that are being transported

449   from low levels (Rosenfeld et al., 2008), as suggested by the increased latent heating associated

450   with the ice phase processes (Fig. 16d). But this is not the major mechanism for the large aerosol

451   effects on convective intensity in this case.

452   Note that both ACI and ARI are considered in the aerosol effects we discussed above,

453   and the results above suggest ACI plays a key role in invigorating convection. To confirm that,

454   we conducted two additional sensitivity tests by turning off ARI based on LandAero and

455   No_Aero, referred to as LandAero_ACI and No_Aero_ACI, respectively. The differences in

456   precipitation and convective intensity between LandAero_ACI and No_Aero_ACI (i.e., ACI

457   effect) are only slightly smaller than the differences between LandAero and No_Aero (i.e., the

458   total aerosol effect). This confirms that ACI is the major factor responsible for the convective

459   invigoration and precipitation enhancement by aerosols.

460   **4 Conclusions and discussion**

461   We have investigated the Houston urbanization effects on convective evolution,

462   convective intensity, and precipitation of a sea-breeze induced convective storm using the WRF-

463   Chem coupled with SBM and the BEM-BEP urban canopy model. The baseline simulation with

464   the urbanization effects considered was extensively evaluated in Zhang et al. (2020) in aerosol

465   and CCN, surface meteorological measurements, reflectivity and precipitation, and in this study

466   in Houston cell reflectivity and precipitation. The simulated convective storm in Houston was

467   shown to be consistent with the observed maximal radar reflectivity and peak precipitation

468   intensity and PDF, despite the peak precipitation time was about ~40 min earlier. The

469   accumulated rain is overestimated by the baseline simulation due to the longer rain period.

470   Model sensitivity tests were carried out to examine the joint and respective effects of

471   urban land and anthropogenic aerosols as a result of Houston urbanization on convective

472   evolution and precipitation. We find that the joint effect of Houston urban land and

473   anthropogenic aerosols enhances the storm intensity (by ~60% in the mean of top 25 percentiles

474   in deep cloud stage), radar reflectivity (by up to 10 dBZ), peak precipitation rate (by ~ 45%), and

475   the accumulated rain (by ~ 26%), with the anthropogenic aerosol effect more significant than the

476   urban land effect overall. The anthropogenic aerosol effect increases the peak precipitation rate

477   by ~ 30% and the frequency of large rain rates (> 15 mm h^{-1} by about 5 times). Although urban

478   land effect alone (under the condition of existence of anthropogenic aerosols) does not impact

479   the peak precipitation rate and the frequency of large rain rates much, its interaction with aerosol

480   effects leads to an increase in the peak rain rates by 45% and the frequency of large rain rates by

481   an order of magnitudes. Therefore, the interactions between the two factors amplify the effect on

482   precipitation, particularly on the large rain rates, emphasizing the importance of considering both

483   effects in studying urbanization effects on convective clouds and precipitation.

484   The Houston urban land effect affects the convective evolution, making the initiation of

485   mixed-phase cloud and surface rain ~30 min earlier because of the strengthened sea breeze

486   circulation as a result of urban heating. It also slows down the dissipation of convective storm

487   because the urban heating extends to late afternoon and evening. The aerosol effect from

488   Houston anthropogenic emissions overall invigorates convection and precipitation, with ACI

489   dominant. The ACI effect is mainly through enhanced condensation (so-called "warm-phase

490   invigoration") by activating numerous small aerosol particles at higher levels above the cloud

491   base. This invigoration is notable starting from the mixed-phase cloud stage and becomes more

492   significant at the deep cloud stage. The enhanced convective intensity in the mixed-phase cloud

493   stage by aerosols accelerates the development of convective storm into the deep cloud stage by ~

494   40 min, which is significant for thunderstorms since the storm duration is only a few hours.

495   This study improves our understanding of how Houston urban land and anthropogenic

496   aerosols jointly shape thunderstorms in the region. Our findings of the relative importance of

497   urban land effect versus anthropogenic aerosol effects are consistent with some of the previous

498   studies, which showed that for coastal cities, the anthropogenic aerosol effect on precipitation

499   was relatively more important than the urban land effect (Liu and Niyogi et al., 2019; Ganeshan

500   et al., 2013; Ochoa et al., 2015, Hu et al. 2019b). The low background aerosol concentration in

501   coastal cities is one of the factors responsible for the significant aerosol effect. In Houston,

502   another factor would be the warm and humid meteorological conditions, in which aerosols were

503   shown to invigorate convective clouds in many previous studies as reviewed in Tao et al. (2012)

504   and Fan et al. (2016).

505   For simulating aerosol-deep convective cloud interactions, there are a few key modeling

506   requirements as summarized in Fan et al. (2016), such as (1) the prognostic supersaturation is

507   needed for secondary aerosol activation, condensation, and evaporation calculations, (2)

508   hydrometeor size distributions need to be prognostic to physically simulate the responses of

509   microphysical processes to CCN changes, and (3) aerosols need to be prognostic, and fixed

510   aerosol concentrations gave unrealistic cloud properties and qualitatively changed aerosol

511   impacts on convective intensity (Fan et al., 2012). With thee SBM used in this study, all these

512 criteria are satisfied. Furthermore, for (3), we are not only prognosing aerosol numbers but also

513 aerosol composition and size distribution by coupling the SBM with the chemistry and aerosol

514 components. With this coupling, the spatial heterogeneity of aerosols is considered. Also, aerosol

515 regeneration and wet removal processes can be more physically accounted for compared with the

516 WRF-Chem with two-moment bulk schemes (Gao et al., 2016). The spatial heterogeneity of

517 aerosols was shown to play an important role in simulating a torrential rain event observed over

518 Seoul, Korea (Lee et al., 2018). However, bin schemes also have uncertainties in representing

519 ice-related processes mainly due to our poor understanding of convective microphysics such as

520 ice nucleation and riming processes. In particular, the conversions between different ice

521 categories are also determined by threshold sizes or masses. However, those uncertainties are not

522 expected to qualitatively change the warm-phase invigoration mechanism which occurs via

523 enhanced condensation. In the companion paper Zhang et al. (2020), we carried out a small

524 number of ensemble simulations for the anthropogenic aerosol effects for the same case and the

525 results are consistent with this study, indicating this mechanism is robust with the initial

526 thermodynamic and dynamic perturbations. More sophisticated uncertainty qualifications can be

527 done in future with a larger number of ensembles when computer power becomes more

528 advanced.

529   The finding that urban land effect enhances sea breeze circulation, which transports more

530 moisture into the urban area and enhances convection and precipitation, is consistent with

531 previous studies, such as Ryu et al. (2016) for the Baltimore–Washington metropolitan area, and

532 You et al. (2019) for the Pearl River Delta (PRD) region.

533

534 **Acknowledgment**

535   This study is supported by the U.S. Department of Energy Office of Science Early Career

536   Award Program. PNNL is operated for the U.S. Department of Energy (DOE) by Battelle

537   Memorial Institute under contract DE-AC05-76RL01830. This research used resources of the

538   PNNL Institutional Computing (PIC), and National Energy Research Scientific Computing

539   Center (NERSC), a U.S. Department of Energy Office of Science User Facility operated under

540   Contract No. DE-AC02-05CH11231. The original simulation data will be available through the

541   NERSC data repository after the paper is accepted.

542

543 **Reference**

544 Alig, R. J., Kline, J. D., and Lichtenstein, M.: Urbanization on the US landscape: looking ahead in

545   the 21st century, Landscape Urban Plan, 69, 219-234, doi:

546   10.1016/j.landurbplan.2003.07.004, 2004.

547 Angevine, W. M., Tjernstrom, M., and Zagar, M.: Modeling of the coastal boundary layer and

548   pollutant transport in New England, J Appl Meteorol Clim, 45, 137-154, doi:

549   10.1175/Jam2333.1, 2006.

550 Ashley, W. S., Bentley, M. L., and Stallins, J. A.: Urban-induced thunderstorm modification in the

551   Southeast United States, Climatic Change, 113, 481-498, doi: 10.1007/s10584-011-0324-

552   1, 2012.

553 Banta, R. M., Senff, C. J., Nielsen-Gammon, J., Darby, L. S., Ryerson, T. B., Alvarez, R. J.,

554   Sandberg, S. R., Williams, E. J., and Trainer, M.: A bad air day in Houston, B Am Meteorol

555   Soc, 86, 657-669, doi: 10.1175/Bams-86-5-657, 2005.

556 Bao, J. W., Michelson, S. A., McKeen, S. A., and Grell, G. A.: Meteorological evaluation of a
557   weather-chemistry forecasting model using observations from the TEXAS AQS 2000 field
558   experiment, J Geophys Res-Atmos, 110, D21105, doi: 10.1029/2004jd005024, 2005.

559 Bornstein, R., and Lin, Q. L.: Urban heat islands and summertime convective thunderstorms in
560   Atlanta: three case studies, Atmos Environ, 34, 507-516, doi: 10.1016/S1352-
561   2310(99)00374-X, 2000.

562 Caicedo, V., Rappenglueck, B., Cuchiara, G., Flynn, J., Ferrare, R., Scarino, A. J., Berkoff, T.,
563   Senff, C., Langford, A., and Lefer, B.: Bay Breeze and Sea Breeze Circulation Impacts on
564   the Planetary Boundary Layer and Air Quality From an Observed and Modeled
565   DISCOVER-AQ Texas Case Study, J Geophys Res-Atmos, 124, 7359-7378, doi:
566   10.1029/2019jd030523, 2019.

567 Carrio, G. G., Cotton, W. R., and Cheng, W. Y. Y.: Urban growth and aerosol effects on convection
568   over Houston Part I: The August 2000 case, Atmos Res, 96, 560-574, doi:
569   10.1016/j.atmosres.2010.01.005, 2010.

570 Chen, F., Miao, S. G., Tewari, M., Bao, J. W., and Kusaka, H.: A numerical study of interactions
571   between surface forcing and sea breeze circulations and their effects on stagnation in the
572   greater Houston area, J Geophys Res-Atmos, 116, D12105, doi: 10.1029/2010jd015533,
573   2011.

574 Greene, D.R. and Clark, R.A.: Vertically Integrated Liquid Water - New Analysis Tool. Mon. Wea.
575   Rev. 100, 548, 1972.

576 Fan, J. W., Zhang, R. Y., Li, G. H., and Tao, W. K.: Effects of aerosols and relative humidity on
577   cumulus clouds, J Geophys Res-Atmos, 112, D14204, doi: 10.1029/2006jd008136, 2007.

578   Fan, J. W., Leung, L. R., Li, Z. Q., Morrison, H., Chen, H. B., Zhou, Y. Q., Qian, Y., and Wang,

579   Y.: Aerosol impacts on clouds and precipitation in eastern China: Results from bin and

580   bulk microphysics, J Geophys Res-Atmos, 117, D00k36, doi: 10.1029/2011jd016537,

581   2012.

582   Fan, J. W., Leung, L. R., Rosenfeld, D., Chen, Q., Li, Z. Q., Zhang, J. Q., and Yan, H. R.:

583   Microphysical effects determine macrophysical response for aerosol impacts on deep

584   convective clouds, P Natl Acad Sci USA, 110, E4581-E4590, doi:

585   10.1073/pnas.1316830110, 2013.

586   Fan, J. W., Liu, Y. C., Xu, K. M., North, K., Collis, S., Dong, X. Q., Zhang, G. J., Chen, Q., Kollias,

587   P., and Ghan, S. J.: Improving representation of convective transport for scale-aware

588   parameterization: 1. Convection and cloud properties simulated with spectral bin and bulk

589   microphysics, J Geophys Res-Atmos, 120, 3485-3509, doi: 10.1002/2014jd022142, 2015.

590   Fan, J. W., Wang, Y., Rosenfeld, D., and Liu, X. H.: Review of Aerosol-Cloud Interactions:

591   Mechanisms, Significance, and Challenges, J Atmos Sci, 73, 4221-4252, doi: 10.1175/Jas-

592   D-16-0037.1, 2016.

593   Fan, J. W., Han, B., Varble, A., Morrison, H., North, K., Kollias, P., Chen, B. J., Dong, X. Q.,

594   Giangrande, S. E., Khain, A., Lin, Y., Mansell, E., Milbrandt, J. A., Stenz, R., Thompson,

595   G., and Wang, Y.: Cloud-resolving model intercomparison of an MC3E squall line case:

596   Part I-Convective updrafts, J Geophys Res-Atmos, 122, 9351-9378, doi:

597   10.1002/2017jd026622, 2017.

598   Fan, J. W., Rosenfeld, D., Zhang, Y. W., Giangrande, S. E., Li, Z. Q., Machado, L. A. T., Martin,

599   S. T., Yang, Y., Wang, J., Artaxo, P., Barbosa, H. M. J., Braga, R. C., Comstock, J. M.,

600   Feng, Z., Gao, W. H., Gomes, H. B., Mei, F., Pohlker, C., Pohlker, M. L., Poschl, U., and

601   de Souza, R. A. F.: Substantial convection and precipitation enhancements by ultrafine

602   aerosol particles, Science, 359, 411-418, doi: 10.1126/science.aan8461, 2018.

603 Fast, J. D., Gustafson, W. I., Easter, R. C., Zaveri, R. A., Barnard, J. C., Chapman, E. G., Grell, G.

604   A., and Peckham, S. E.: Evolution of ozone, particulates, and aerosol direct radiative

605   forcing in the vicinity of Houston using a fully coupled meteorology-chemistry-aerosol

606   model, J Geophys Res-Atmos, 111, D21305, doi: 10.1029/2005jd006721, 2006.

607 Ganeshan, M., Murtugudde, R., and Imhoff, M. L.: A multi-city analysis of the UHI-influence on

608   warm season rainfall, 6, 1-23, doi: 10.1016/j.uclim.2013.09.004, 2013.

609 Gao, W. H., Fan, J. W., Easter, R. C., Yang, Q., Zhao, C., and Ghan, S. J.: Coupling spectral-bin

610   cloud microphysics with the MOSAIC aerosol model in WRF-Chem: Methodology and

611   results for marine stratocumulus clouds, J Adv Model Earth Sy, 8, 1289-1309, doi:

612   10.1002/2016ms000676, 2016.

613 Gelaro, R., McCarty, W., Suarez, M. J., Todling, R., Molod, A., Takacs, L., Randles, C. A.,

614   Darmenov, A., Bosilovich, M. G., Reichle, R., Wargan, K., Coy, L., Cullather, R., Draper,

615   C., Akella, S., Buchard, V., Conaty, A., da Silva, A. M., Gu, W., Kim, G. K., Koster, R.,

616   Lucchesi, R., Merkova, D., Nielsen, J. E., Partyka, G., Pawson, S., Putman, W., Rienecker,

617   M., Schubert, S. D., Sienkiewicz, M., and Zhao, B.: The Modern-Era Retrospective

618   Analysis for Research and Applications, Version 2 (MERRA-2), J Climate, 30, 5419-5454,

619   doi: 10.1175/Jcli-D-16-0758.1, 2017.

620 Grabowski, W. W., and H. Morrison: Do ultrafine cloud condensation nuclei invigorate deep

621   convection? J. Atmos. Sci., 77(7), 2567-2583, doi: 10.1175/JAS-D-20-0012.1, 2020.

622 Grell, G. A., Peckham, S. E., Schmitz, R., McKeen, S. A., Frost, G., Skamarock, W. C., and Eder,

623   B.: Fully coupled "online" chemistry within the WRF model, Atmos Environ, 39, 6957-

624   6975, doi: 10.1016/j.atmosenv.2005.04.027, 2005.

625 Guenther, A., Karl, T., Harley, P., Wiedinmyer, C., Palmer, P. I., and Geron, C.: Estimates of

626   global terrestrial isoprene emissions using MEGAN (Model of Emissions of Gases and

627   Aerosols from Nature), Atmos Chem Phys, 6, 3181-3210, doi: 10.5194/acp-6-3181-2006,

628   2006.

629 Haberlie, A. M., Ashley, W. S., and Pingel, T. J.: The effect of urbanisation on the climatology of

630   thunderstorm initiation, Q J Roy Meteor Soc, 141, 663-675, doi: 10.1002/qj.2499, 2015.

631 Hu, J. X., Rosenfeld, D., Zrnic, D., Williams, E., Zhang, P. F., Snyder, J. C., Ryzhkov, A.,

632   Hashimshoni, E., Zhang, R. Y., and Weitz, R.: Tracking and characterization of convective

633   cells through their maturation into stratiform storm elements using polarimetric radar and

634   lightning detection, Atmos Res, 226, 192-207, doi: 10.1016/j.atmosres.2019.04.015, 2019a.

635 Hu, J. X., Rosenfeld, D., Ryzhkov, A., Zrnic, D., Williams, E., Zhang, P. F., Snyder, J. C., Zhang,

636   R. Y., and Weitz, R.: Polarimetric Radar Convective Cell Tracking Reveals Large

637   Sensitivity of Cloud Precipitation and Electrification Properties to CCN, J Geophys Res-

638   Atmos, 124, 12194-12205, doi: 10.1029/2019jd030857, 2019b.

639 Hubbart, J. A., Kellner, E., Hooper, L., Lupo, A. R., Market, P. S., Guinan, P. E., Stephan, K., Fox,

640   N. I., and Svoma, B. M.: Localized Climate and Surface Energy Flux Alterations across an

641   Urban Gradient in the Central US, Energies, 7, 1770-1791, doi: 10.3390/en7031770, 2014.

642 Kar, S. K., and Liou, Y. A.: Influence of Land Use and Land Cover Change on the Formation of

643   Local Lightning, Remote Sens-Basel, 11, 407, doi: 10.3390/rs11040407, 2019.

644 Khain, A., Pokrovsky, A., Pinsky, M., Seifert, A., and Phillips, V.: Simulation of effects of

645   atmospheric aerosols on deep turbulent convective clouds using a spectral microphysics

646   mixed-phase cumulus cloud model. Part I: Model description and possible applications, J

647   Atmos Sci, 61, 2963-2982, doi: 10.1175/Jas-3350.1, 2004.

648 Khain, A. P., Beheng, K. D., Heymsfield, A., Korolev, A., Krichak, S. O., Levin, Z., Pinsky, M.,

649   Phillips, V., Prabhakaran, T., Teller, A., van den Heever, S. C., and Yano, J. I.:

650   Representation of microphysical processes in cloud-resolving models: Spectral (bin)

651   microphysics versus bulk parameterization, Rev Geophys, 53, 247-322, doi:

652   10.1002/2014rg000468, 2015.

653 Kingfield, D.M., K.M., Calhoun, and K.M., de Beurs: Antenna structures and cloud-to-ground

654   lightning location: 1995–2015, Geophys. Res. Lett., 44, 5203–5212,

655   doi:10.1002/2017gl073449, 2017.

656 Kocen, M.: Observations of sea-breeze fronts along the houston gulf coast, University of Houston,

657   University of Houston libraries, http://hdl.handle.net/10657/864, 76pp., 2013.

658 Korolev A., and I. Mazin: Supersaturation of water vapor in clouds. J. Atmos. Sci., 60, 2957-

659   2974, 2003.

660 Lebo, Z.: A Numerical Investigation of the Potential Effects of Aerosol-Induced Warming and

661   Updraft Width and Slope on Updraft Intensity in Deep Convective Clouds, J Atmos Sci,

662   75, 535-554, doi: 10.1175/Jas-D-16-0368.1, 2018.

663 Lee, S. S., Kim, B. G., Li, Z. Q., Choi, Y. S., Jung, C. H., Um, J., Mok, J., and Seo, K. H.: Aerosol

664   as a potential factor to control the increasing torrential rain events in urban areas over the

665   last decades, Atmos Chem Phys, 18, 12531-12550, doi: 10.5194/acp-18-12531-2018, 2018.

Li, Z. Q., Wang, Y., Guo, J. P., Zhao, C. F., Cribb, M. C., Dong, X. Q., Fan, J. W., Gong, D. Y., Huang, J. P., Jiang, M. J., Jiang, Y. Q., Lee, S. S., Li, H., Li, J. M., Liu, J. J., Qian, Y., Rosenfeld, D., Shan, S. Y., Sun, Y. L., Wang, H. J., Xin, J. Y., Yan, X., Yang, X., Yang, X. Q., Zhang, F., and Zheng, Y. T.: East Asian Study of Tropospheric Aerosols and their Impact on Regional Clouds, Precipitation, and Climate (EAST-AIR(CPC)), J Geophys Res-Atmos, 124, 13026-13054, doi: 10.1029/2019jd030758, 2019.

Liu, J., and Niyogi, D.: Meta-analysis of urbanization impact on rainfall modification, Sci Rep-Uk, 9, 7301, doi: 10.1038/s41598-019-42494-2, 2019.

Morrison, H., Curry, J. A., and Khvorostyanov, V. I.: A new double-moment microphysics parameterization for application in cloud and climate models. Part I: Description, J Atmos Sci, 62, 1665-1677, doi: 10.1175/Jas3446.1, 2005.

Niyogi, D., Holt, T., Zhong, S., Pyle, P. C., and Basara, J.: Urban and land surface effects on the 30 July 2003 mesoscale convective system event observed in the southern Great Plains, J Geophys Res-Atmos, 111, D19107, doi: 10.1029/2005jd006746, 2006.

Niyogi, D., Pyle, P., Lei, M., Arya, S. P., Kishtawal, C. M., Shepherd, M., Chen, F., and Wolfe, B.: Urban Modification of Thunderstorms: An Observational Storm Climatology and Model Case Study for the Indianapolis Urban Region, J Appl Meteorol Clim, 50, 1129-1144, doi: 10.1175/2010jamc1836.1, 2011.

Ochoa, C. A., Quintanar, A. I., Raga, G. B., and Baumgardner, D.: Changes in Intense Precipitation Events in Mexico City, J Hydrometeorol, 16, 1804-1820, doi: 10.1175/Jhm-D-14-0081.1, 2015.

Pinsky M., I.P. Mazin, A. Korolev, and A.P. Khain: Supersaturation and diffusional droplet growth in liquid clouds. J. Atmos. Sci. 70, 2778-2793, 2013.

689 Rosenfeld, D., Lohmann, U., Raga, G. B., O'Dowd, C. D., Kulmala, M., Fuzzi, S., Reissell, A.,

690   and Andreae, M. O.: Flood or drought: How do aerosols affect precipitation?, Science, 321,

691   1309-1313, doi: 10.1126/science.1160606, 2008.

692 Rosenfeld D, and Coauthors: Global observations of aerosol-cloud-precipitation-climate

693   interactions. Rev. Geophys., 52, 750–808, doi:10.1002/2013RG000441, 2014.

694 Ryu, Y. H., Smith, J. A., Bou-Zeid, E., and Baeck, M. L.: The Influence of Land Surface

695   Heterogeneities on Heavy Convective Rainfall in the Baltimore-Washington Metropolitan

696   Area, Mon Weather Rev, 144, 553-573, doi: 10.1175/Mwr-D-15-0192.1, 2016.

697 Sarangi, C., Tripathi, S. N., Qian, Y., Kumar, S., and Leung, L. R.: Aerosol and Urban Land Use

698   Effect on Rainfall Around Cities in Indo-Gangetic Basin From Observations and Cloud

699   Resolving Model Simulations, J Geophys Res-Atmos, 123, 3645-3667, doi:

700   10.1002/2017jd028004, 2018.

701 Schmid, P. E., and Niyogi, D.: Modeling Urban Precipitation Modification by Spatially

702   Heterogeneous Aerosols, J Appl Meteorol Clim, 56, 2141-2153, doi: 10.1175/Jamc-D-16-

703   0320.1, 2017.

704 Sheffield, A. M., Saleeby, S. M., and van den Heever, S. C.: Aerosol-induced mechanisms for

705   cumulus congestus growth, J Geophys Res-Atmos, 120, 8941-8952, doi:

706   10.1002/2015jd023743, 2015.

707 Shen, L. X., Zhao, C. F., Ma, Z. S., Li, Z. Q., Li, J. P., and Wang, K. C.: Observed decrease of

708   summer sea-land breeze in Shanghai from 1994 to 2014 and its association with

709   urbanization, Atmos Res, 227, 198-209, doi: 10.1016/j.atmosres.2019.05.007, 2019.

710 Shephard, J. M.: A review of current investigations of urban-induced rainfall and

711   recommmendations for the future, Earth Interact, 9, doi: 10.1175/EI156.1, 2005.

712   Shepherd, J. M., Pierce, H., and Negri, A. J.: Rainfall modification by major urban areas:

713   Observations from spaceborne rain radar on the TRMM satellite, J Appl Meteorol, 41, 689-

714   701, doi: 10.1175/1520-0450(2002)041<0689:Rmbmua>2.0.Co;2, 2002.

715   Shepherd J.M., J.A. Stallins, M. Jin, T.L. Mote: Urbanization: impacts on clouds, precipitation,

716   and lightning. Monograph on Urban Ecological Ecosystems. Eds. Jacqueline Peterson and

717   Astrid Volder. American Society of Agronomy-Crop Science Society of America- Soil

718   Science Society of America, pp. 354, 2010.

719   Shimadera, H., Kondo, A., Shrestha, K. L., Kitaoka, K., and Inoue, Y.: Numerical Evaluation of

720   the Impact of Urbanization on Summertime Precipitation in Osaka, Japan, Adv Meteorol,

721   379361, doi: 10.1155/2015/379361, 2015.

722   Skamarock, W. C., Klemp, J. B., Dudhia, J., Gill, D. O., Barker, D. M., Duda, M., Huang, X. Y.,

723   Wang, W., and Powers, J. G.: A description of the advanced research WRF version 3,

724   NCAR, Tech. Note, Mesoscale and Microscale Meteorology Division, National Center for

725   Atmospheric Research, Boulder, Colorado, USA, 2008.

726   Tao, W. K., Chen, J. P., Li, Z. Q., Wang, C., and Zhang, C. D.: Impact of Aerosols on Convective

727   Clouds and Precipitation, Rev Geophys, 50, Rg2001, doi: 10.1029/2011rg000369, 2012.

728   Van Den Heever, S. C., and Cotton, W. R.: Urban aerosol impacts on downwind convective storms,

729   J Appl Meteorol Clim, 46, 828-850, doi: 10.1175/Jam2492.1, 2007.

730   Varble, A., Fridlind, A. M., Zipser, E. J., Ackerman, A. S., Chaboureau, J. P., Fan, J. W., Hill, A.,

731   McFarlane, S. A., Pinty, J. P., and Shipway, B.: Evaluation of cloud-resolving model

732   intercomparison simulations using TWP-ICE observations: Precipitation and cloud

733   structure, J Geophys Res-Atmos, 116, D12206, doi: 10.1029/2010jd015180, 2011.

734 Varble, A., Zipser, E. J., Fridlind, A. M., Zhu, P., Ackerman, A. S., Chaboureau, J. P., Fan, J. W.,

735   Hill, A., Shipway, B., and Williams, C.: Evaluation of cloud-resolving and limited area

736   model intercomparison simulations using TWP-ICE observations: 2. Precipitation

737   microphysics, J Geophys Res-Atmos, 119, 13919-13945, doi: 10.1002/2013jd021372,

738   2014.

739 Wiedinmyer, C., Akagi, S. K., Yokelson, R. J., Emmons, L. K., Al-Saadi, J. A., Orlando, J. J., and

740   Soja, A. J.: The Fire INventory from NCAR (FINN): a high resolution global model to

741   estimate the emissions from open burning, Geosci Model Dev, 4, 625-641, doi:

742   10.5194/gmd-4-625-2011, 2011.

743 You, C., Fung, J. C. H., and Tse, W. P.: Response of the Sea Breeze to Urbanization in the Pearl

744   River Delta Region, J Appl Meteorol Clim, 58, 1449-1463, doi: 10.1175/Jamc-D-18-

745   0081.1, 2019.

746 Zaveri, R. A., Easter, R. C., Fast, J. D., and Peters, L. K.: Model for Simulating Aerosol

747   Interactions and Chemistry (MOSAIC), J Geophys Res-Atmos, 113, D13204, doi:

748   10.1029/2007jd008782, 2008.

749 Zhong, S., Qian, Y., Zhao, C., Leung, R., and Yang, X. Q.: A case study of urbanization impact

750   on summer precipitation in the Greater Beijing Metropolitan Area: Urban heat island

751   versus aerosol effects, J Geophys Res-Atmos, 120, 10903-10914, doi:

752   10.1002/2015jd023753, 2015.

753 Zhong, S., Qian, Y., Zhao, C., Leung, R., Wang, H. L., Yang, B., Fan, J. W., Yan, H. P., Yang, X.

754   Q., and Liu, D. Q.: Urbanization-induced urban heat island and aerosol effects on climate

755   extremes in the Yangtze River Delta region of China, Atmos Chem Phys, 17, 5439-5457,

756   doi: 10.5194/acp-17-5439-2017, 2017.

757   Zhang Y., Fan J., Li Z., and Rosenfeld D.: Impacts of Cloud Microphysics Parameterizations on

758   Simulated Aerosol-Cloud-Interactions for Deep Convective Clouds over Houston, Atmos.

759   Chem. Phys. Discuss., https://doi.org/10.5194/acp-2020-372, in review, 2020.

760

761
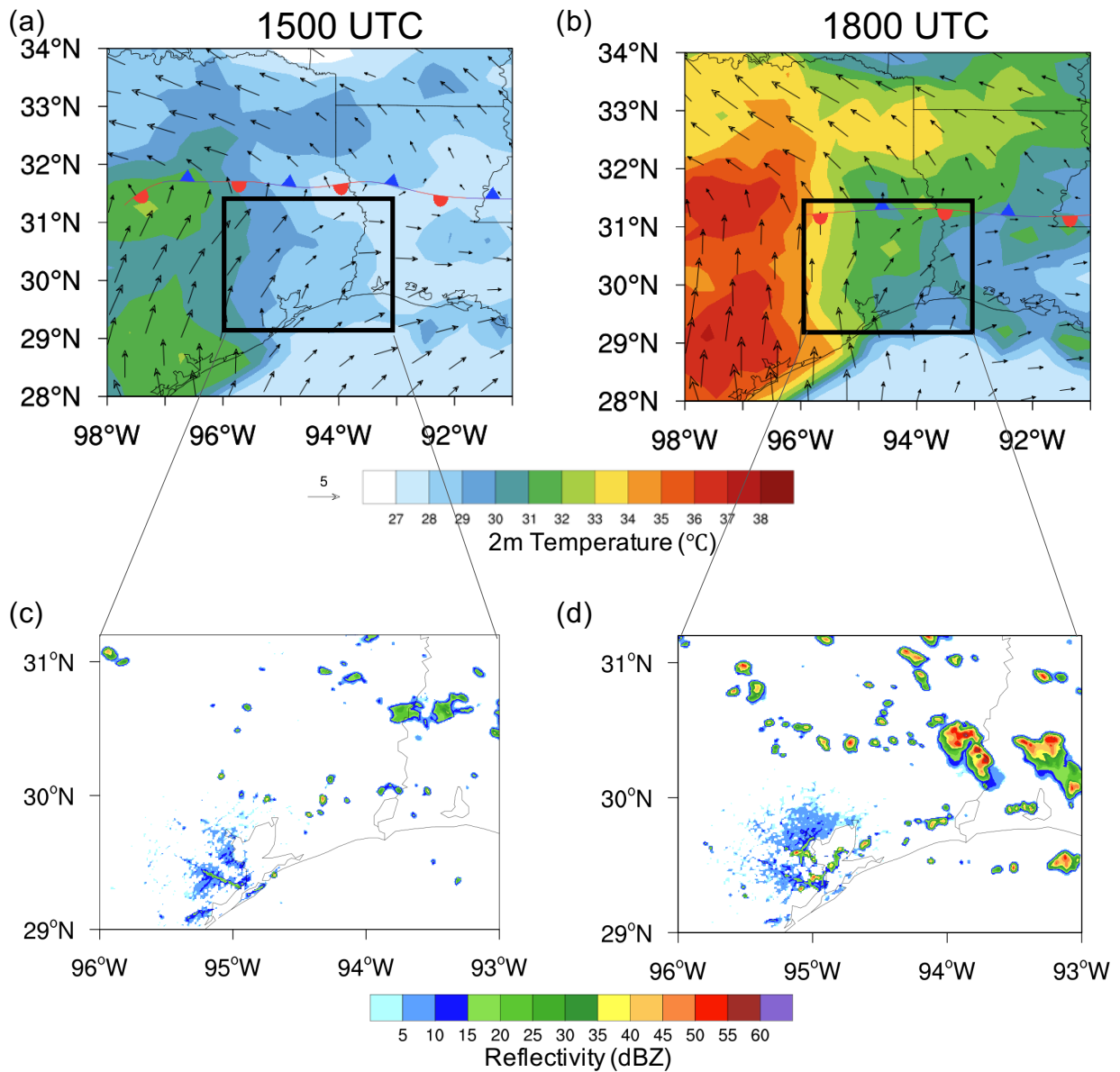
762
763 **Figure 1** (a-b) 2-m Temperature (shaded) and 10-m wind (arrows) from the North American
764 Regional Reanalysis (NARR) reanalysis data (32 km grid spacing), and the stationary front; (c-d)
765 composite reflectivity observed at KHGX (Houston NEXRAD) at 1500 UTC (left) and 1800 UTC
766 (right), 19 Jun 2013.
767
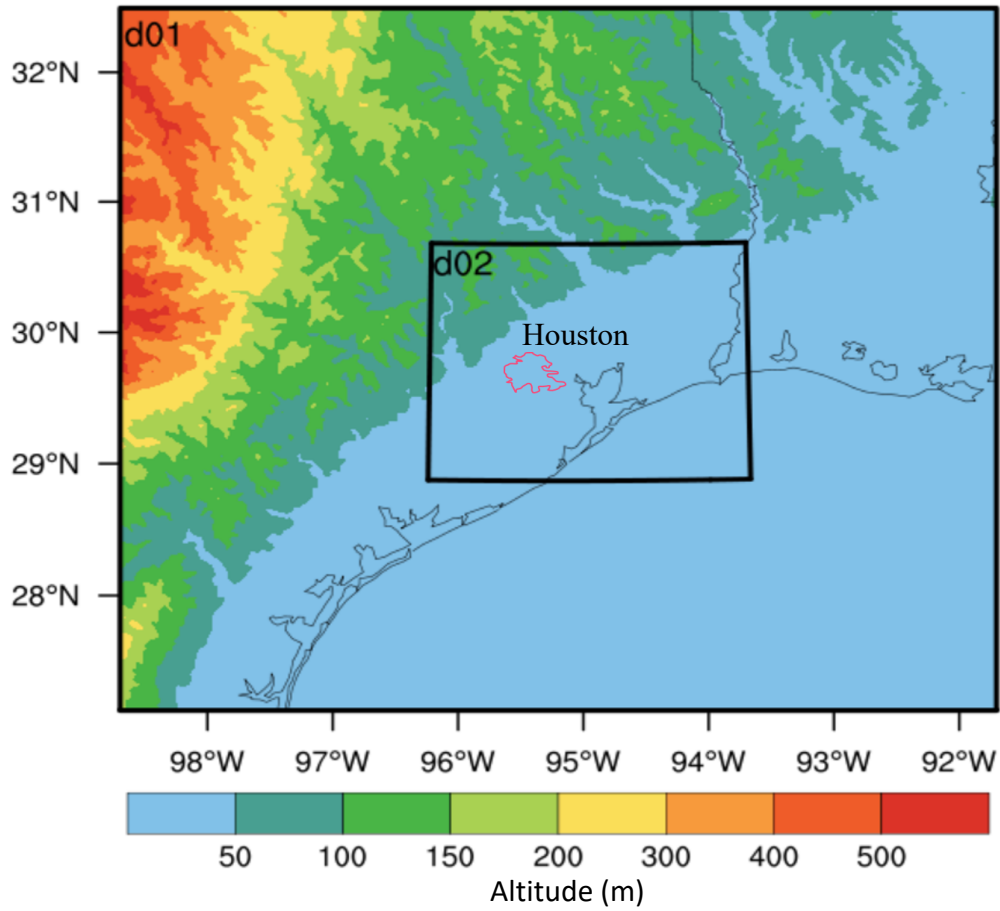
768

769   **Figure 2** The model domain setup. Domain 1 (d01) and Domain 2 (d02) are marked with black

770   boxes. Terrain heights (m) are in color contours. Houston urban area is denoted by a pink

771   contoured line.

772
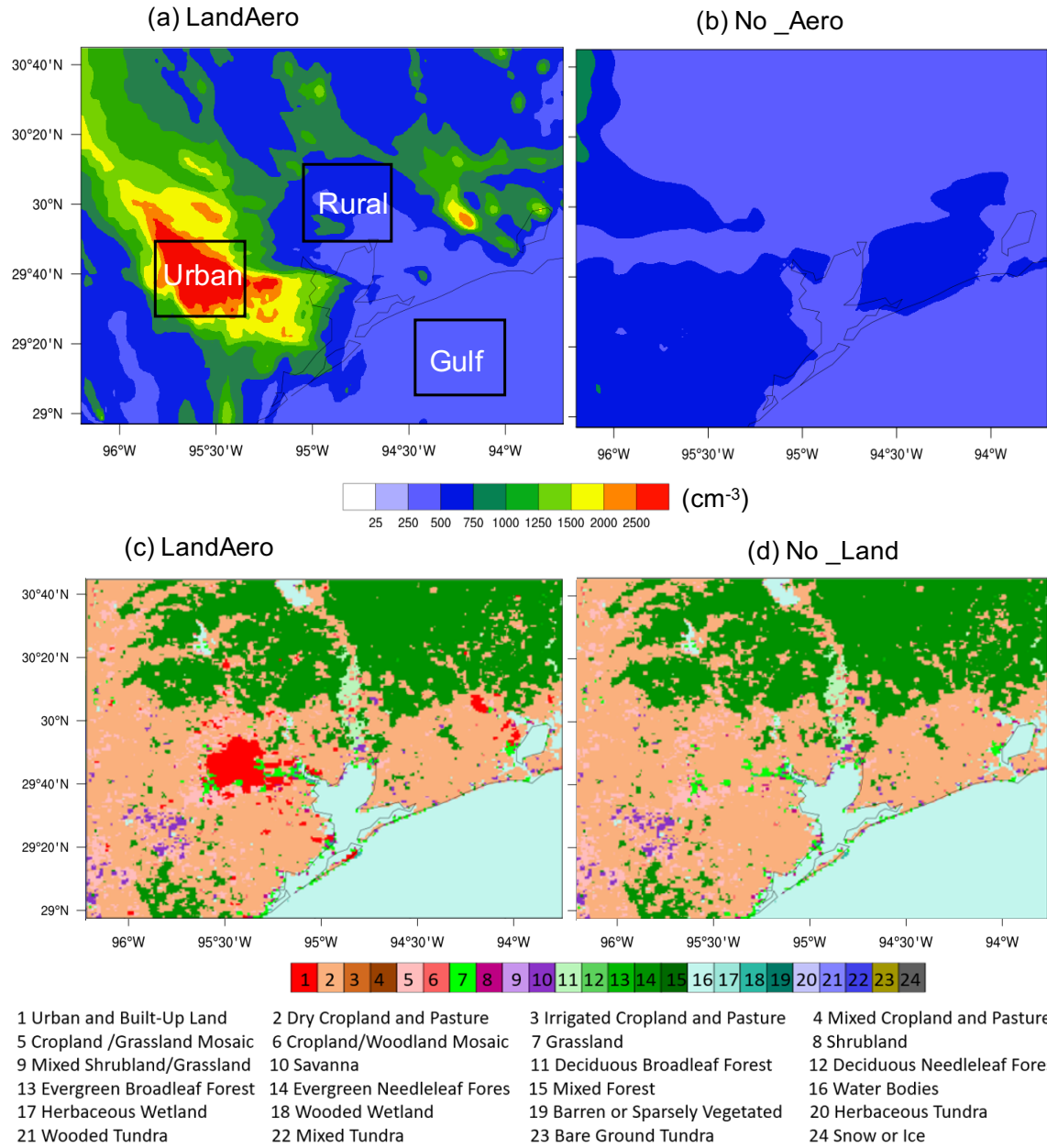
Figure 3 Aerosol number concentration (cm^{-3}) from (a) LandAero (with anthropogenic emission) and (b) No_Aero (with anthropogenic emission turned off) at 1200 UTC, 19 Jun 2013 (6-hr before the convection initiation), and land cover types in (c) LandAero and (d) No_Land.
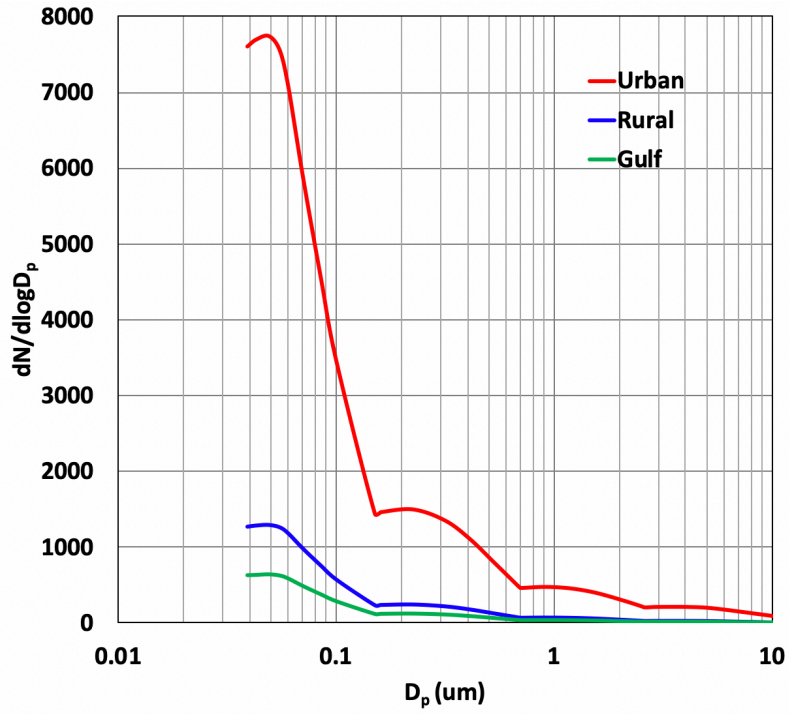
778

779   **Figure 4** Aerosol size distribution over the Urban, Rural, and Gulf of Mexico as marked by three

780   black boxes in Figure 3a from LandAero at 1200 UTC, 19 Jun 2016.

781
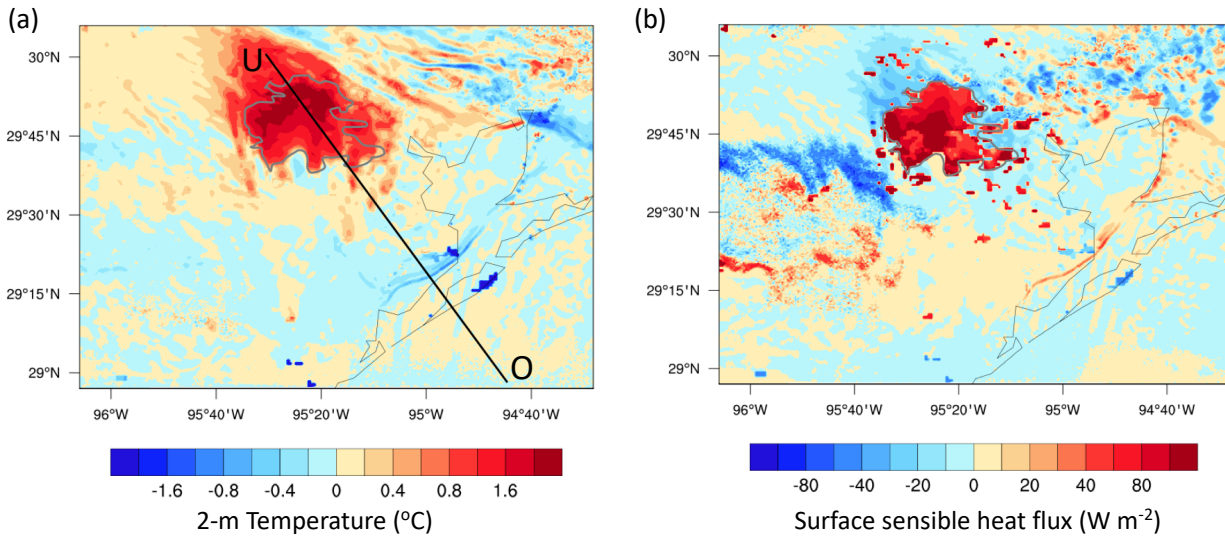
782

783 **Figure 5** Differences of (a) 2-m temperature (°C) and (b) surface sensible heat flux (W m^{-2})

784 between LandAero and No_Land at 1600 UTC 19 Jun 2013. Line UO is where the cross section

785 of sea breeze circulation is examined.

786

787
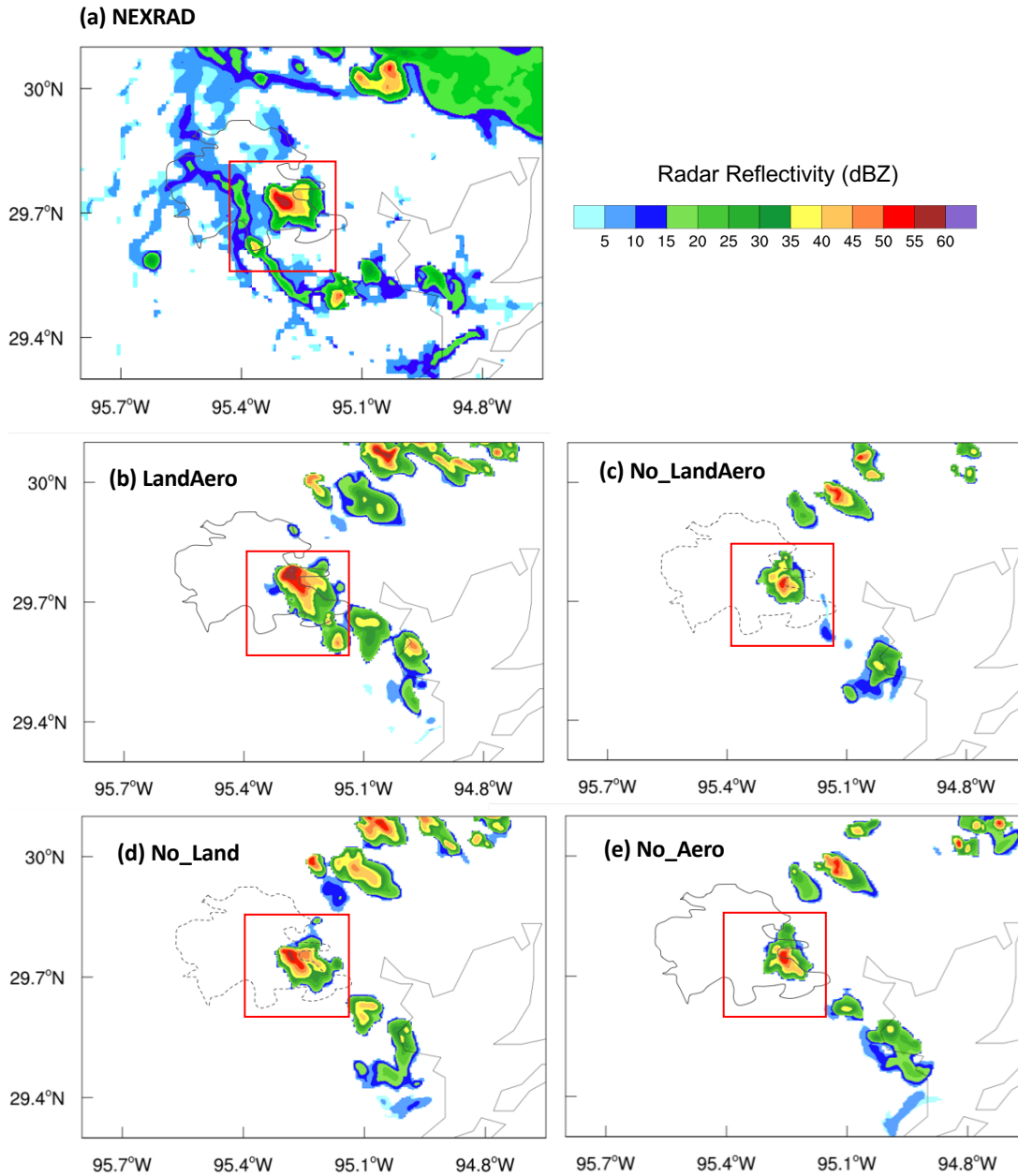
Figure 6 Composite reflectivity (dBZ) from (a) NEXRAD (2217 UTC), (b) LandAero (2140

UTC), (c) No_LandAero (2120 UTC), (d) No_Land (2135 UTC), and (e) No_Aero (2125 UTC)

at the time when the maximal reflectivity of the storm in Houston is reached. Houston city is

marked as dark grey solid contour based on the land cover data shown in Figure 3c. The red box

is the study area for the Houston convective cell.

793

794

795
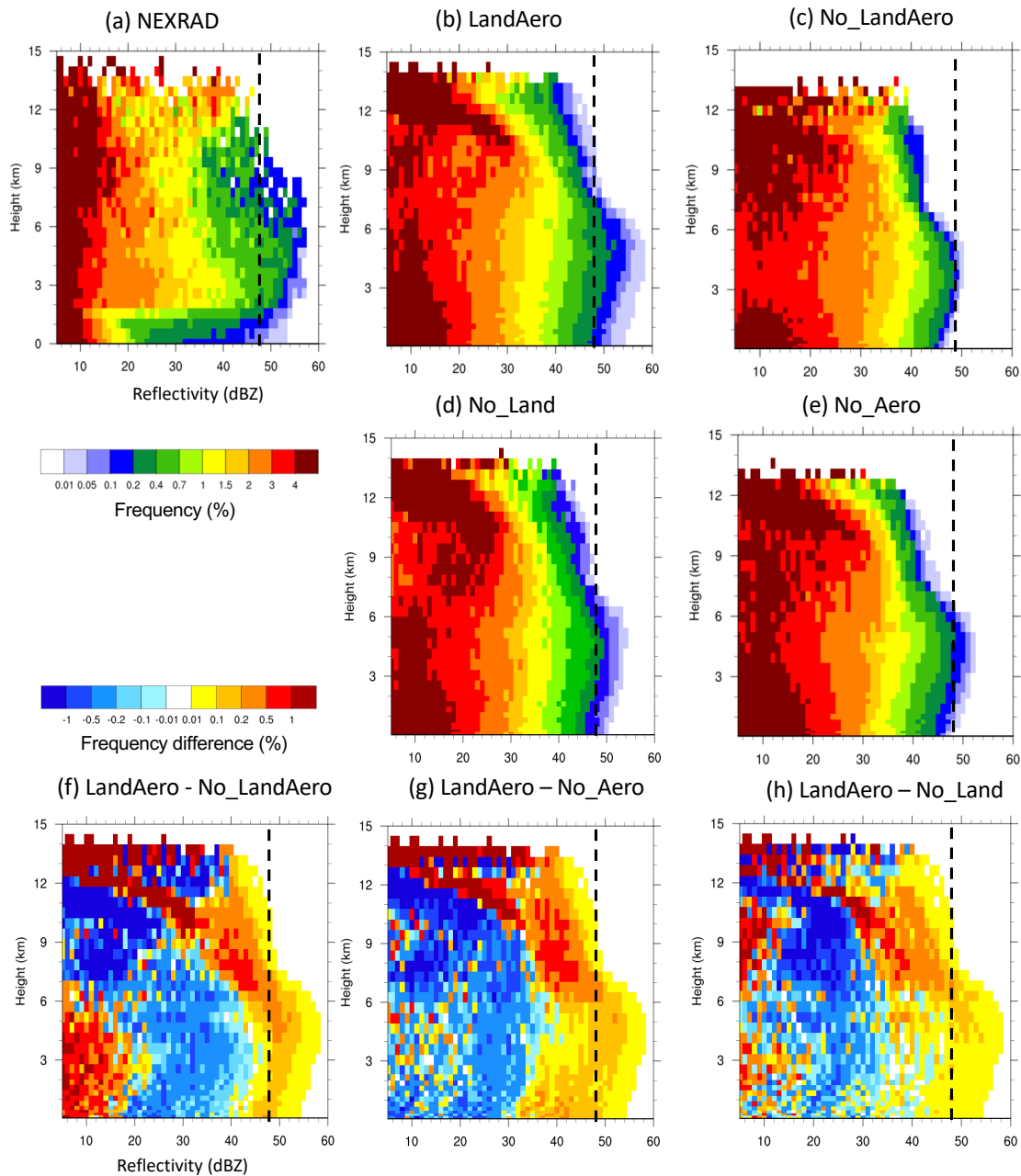
Figure 7 Contoured frequency by altitude diagram (CFAD; %) of reflectivity for the values

larger than 0 dBZ from (a) NEXRAD, (b) LandAero, (c) No_LandAero, (d) No_Land, and (e)

No_Aero. (f-h) present the differences of CFAD (%) of reflectivity for (f) LandAero -

No_LandAero, (g) LandAero - No_Aero, and (h) LandAero - No_Land. Data are from the study

area (red box in Figure 6) over 1800 UTC 19 Jun to 0000 UTC 20 Jun. The vertical dashed line

marks the value for the reflectivity of 48 dBZ.

802
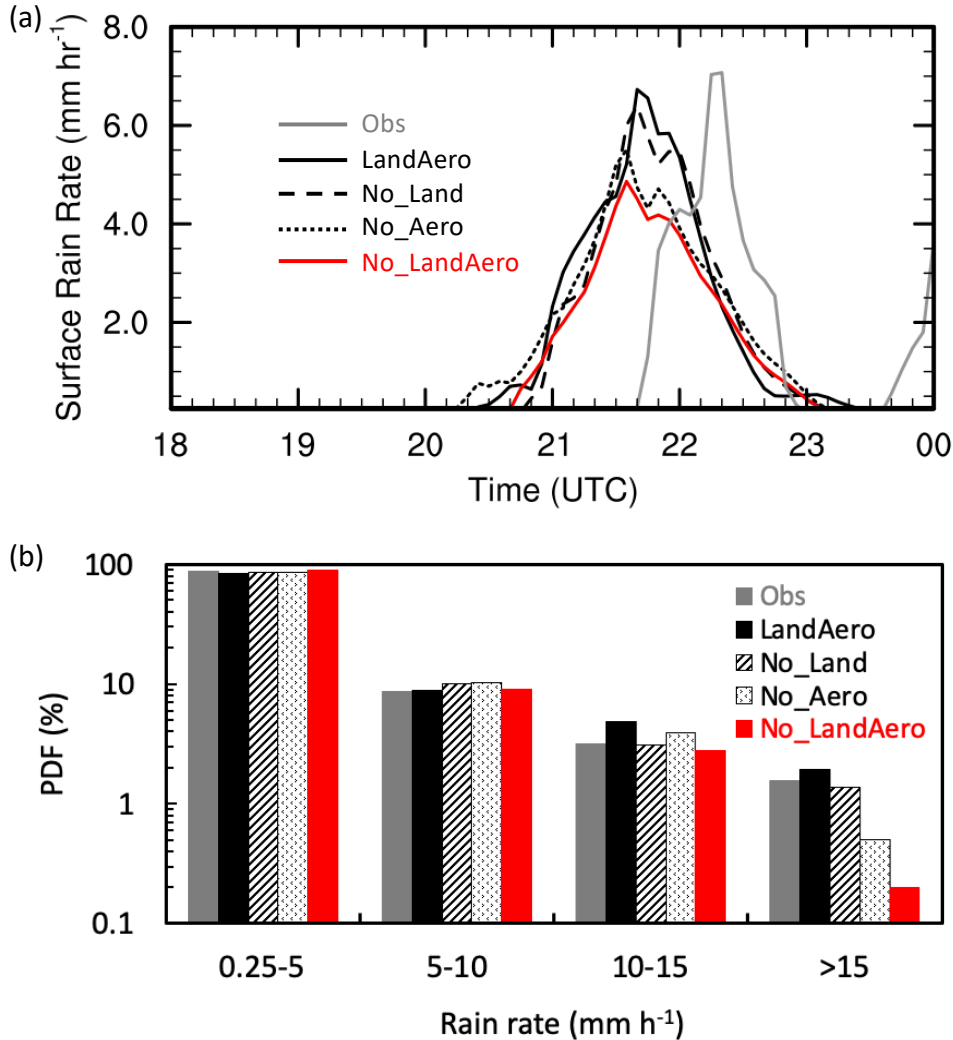
803

804 **Figure 8** (a) Time series of surface rain rate (mm h^{-1}) averaged over the values larger than 0.25

805 mm h^{-1} for the Houston convective cell (red box in Figure 6) and (b) PDFs (%) of rain rates (>

806 0.25 mm h^{-1}) from 1800UTC 19 Jun to 0000 UTC 20 Jun 2013, from Observations, LandAero,

807 No_LandAero, No_Land, and No_Aero. The observation is the NEXRAD retrieved rain rate.

808 Both observation and model data are in every 5-min frequency.
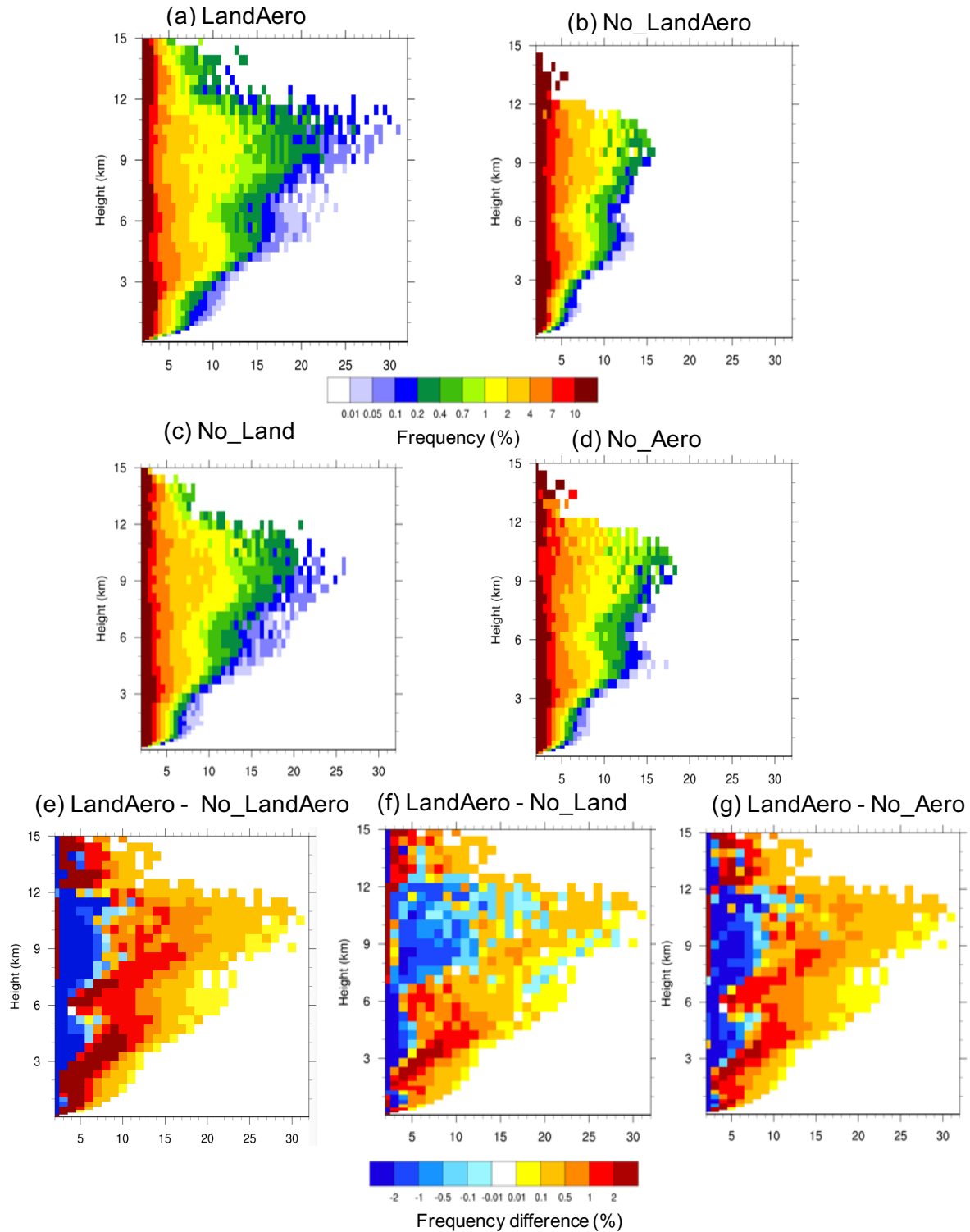
809

810 **Figure 9** CFAD (%) of updraft velocity for values larger than 2 m s⁻¹ from (a) LandAero, (b)

811 LandAero - No_LandAero, (c) LandAero - No_Land, and (d) LandAero - No_Aero over the

812 study area as shown in the red box in Figure 6 during the strong convection periods (60-min

813   duration with 30 min before and after the strongest convection). (e-g) present the differences of

814   CFAD (%) of reflectivity for (e) LandAero - No_LandAero, (f) LandAero -No_Land, and (g)

815   LandAero – No_Aero.

816
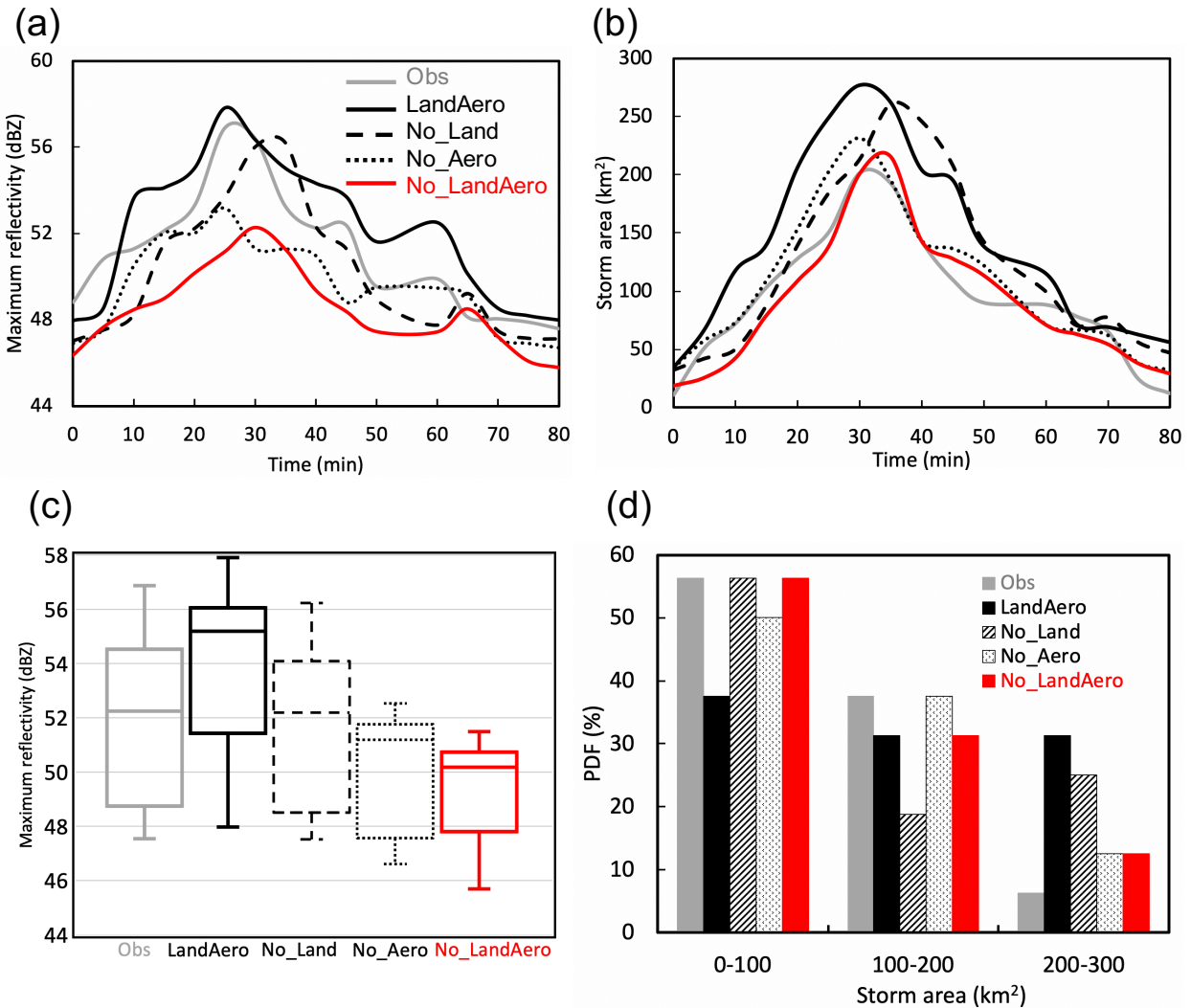
817

818   **Figure 10** Time series of (a) maximum reflectivity (dBZ) and (b) storm area (km^2) for the

819   tracked convective cell from NEXRAD, LandAero, No_LandAero, No_Land, and No_Aero. The

820   time window is from 2140 UTC to 2300 UTC for observations and from 2100 UTC to 2220

821   UTC for model simulations. (c) Box-whisker plots of maximum reflectivity and (d) PDFs of

822   averaged storm areas for the Houston cell from NEXRAD, LandAero, No_LandAero, No_Land,

823   and No_Aero over the respective 80 min time windows as described above. The center line of

824   the box indicates the median value, and the lower (upper) edge of the box indicates the 25th (75th)

825 percentiles. The whiskers indicate the minimum and maximum values. The storm area of the

826 tracked cell is defined as the number of grid points with LWP > 50 g m^{-2} multiplied by the grid

827 box area (0.5 km *0.5 km).

828
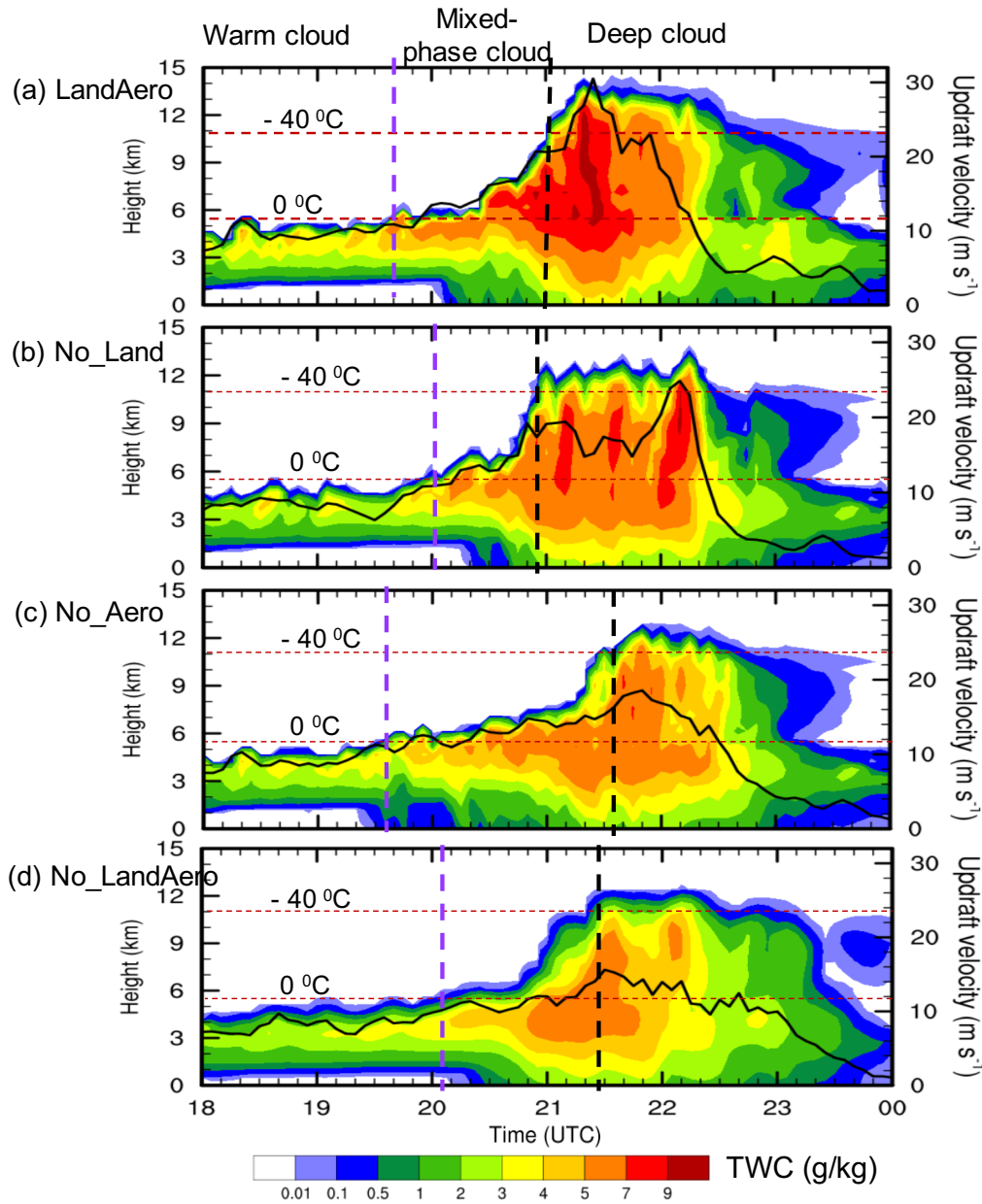
Figure 11 Time series of maximal total water content (shaded; water vapor is not included) and

832 maximal updraft velocity (black line, second y-axis) over the study area as shown in the red box

833 in Figure 6 from LandAero, No_LandAero, No_Land, and No_Aero. Brown horizontal dashed

834   lines denote the freezing level (0 ⁰C) and homogeneous freezing level (-40 ⁰C). The initiation of

835   the mix-phase cloud and deep cloud is denoted by the purple and black vertical dashed lines,

836   respectively.

837

838
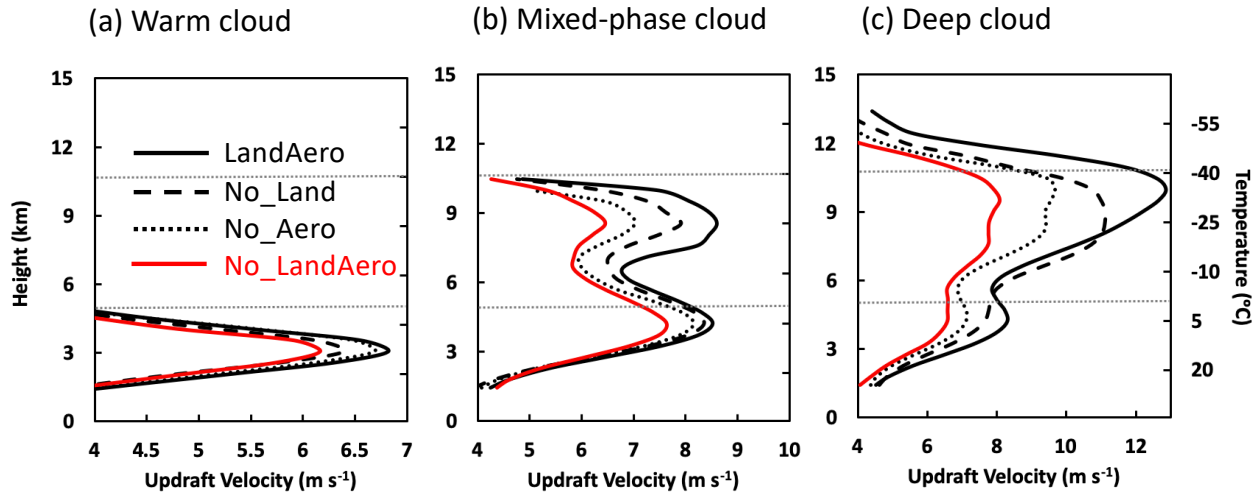
839

840 **Figure 12** Vertical profiles of updraft velocity averaged over the top 25 percentiles (i.e., 75th to

841 100th) of the updrafts with a value greater than 2 m s^{-1} from the simulations LandAero,

842 No_LandAero, No_Land, and No_Aero over the study area at the (a) warm cloud, (b) mixed-

843 phase cloud, and (c) deep cloud stages. The dotted line denotes the freezing level (0 ⁰C).
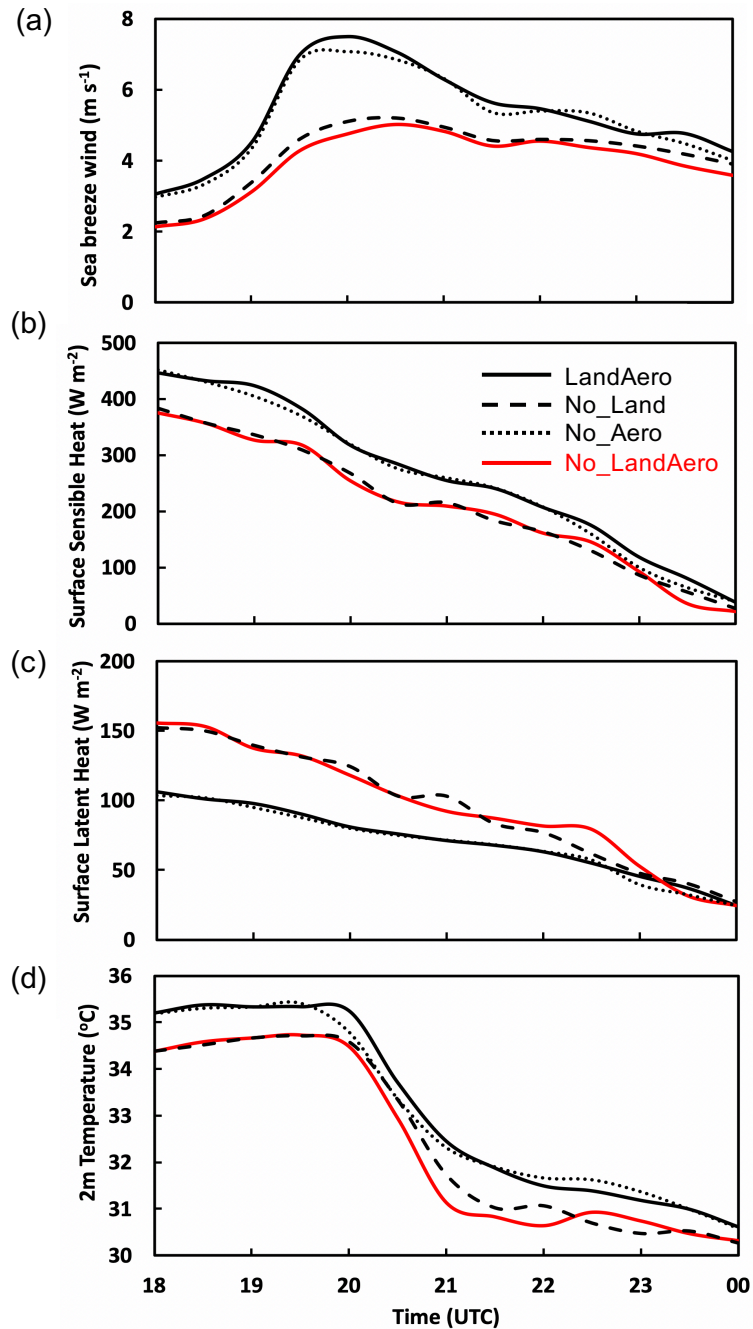
844

845 **Figure 13** Time series of (a) sea breeze wind speed (m s^{-1}), (b) surface sensible heat flux (W m$^-$

846 ^{2}), (c) surface latent heat flux(W m^{-2}), (d) 2-m temperature (°C) from LandAero, No_Land,

847 No_Aero, and No_LandAero. Sea breeze winds are averaged over the horizontal winds along

848 line UO (Figure 5a) from O to U below 1km. Heat fluxes and temperature are averaged over the

849 study area.

850

851
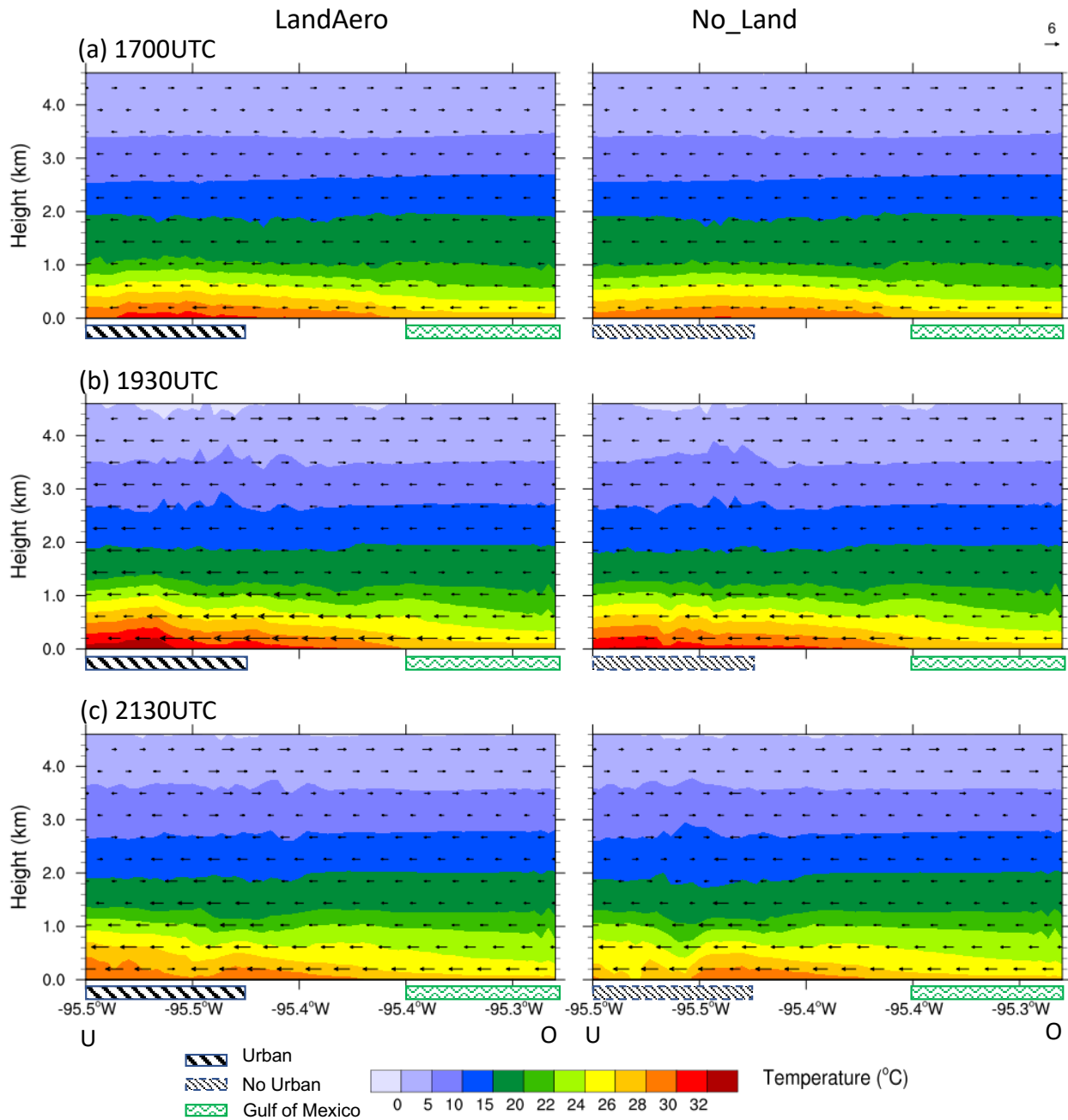
Figure 14 Vertical cross sections of temperature (°C; shaded) and wind vectors (m s^{-1}) along the

line UO in Figure 5a for LandAero (left) and No_Land (right) at (a) 1700, (b) 1930, and (c) 2130

UTC. The bars with stripes and waves on the x-axis represent the urban land and water body in

the Gulf of Mexico, respectively.

856
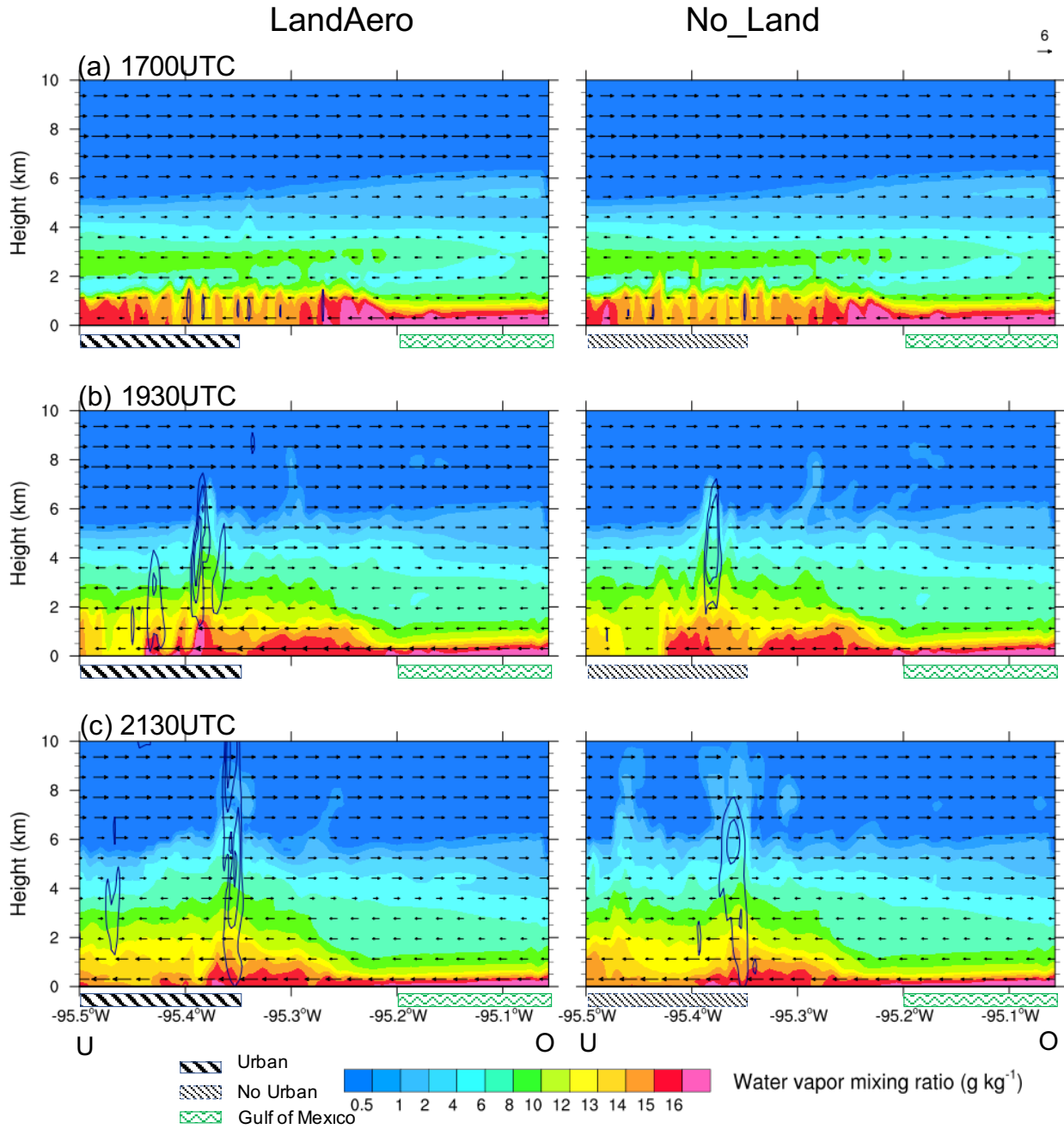
857

858 **Figure 15** Vertical cross sections of water vapor mixing ratio (g kg^{-1}; shaded), updraft velocity

859 (contour lines are 2, 6, and 11 m s^{-1}), and wind vectors along the line UO in Figure 5a for

860 LandAero and No_Land at (a) 1700, (b) 1930, and (c) 2130 UTC.

861
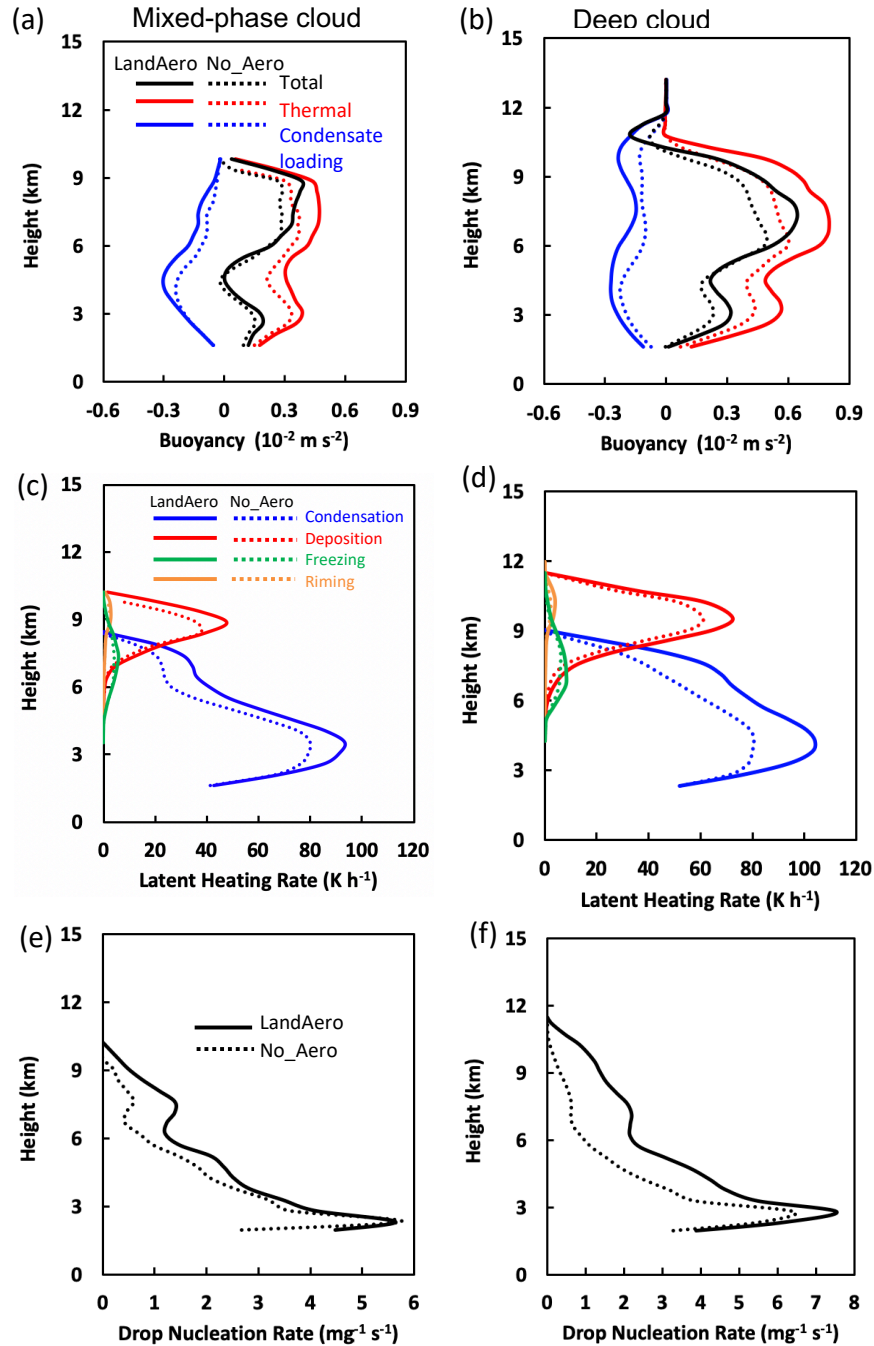
862

863 **Figure 16** Vertical profiles of (a-b) buoyancy terms (m s⁻²; red for Thermal buoyancy, blue for

864 condensate loading and black for total buoyancy), (c-d) latent heating (K h⁻¹) from condensation

865 (blue), deposition (red), drop freezing (orange), and riming (green), and (e-f) droplet nucleation

866 rate (mg⁻¹ s⁻¹) averaged over the top 25 percentiles (i.e., 75th to 100th) of the updrafts with a

867 value greater than 2 m s⁻¹ from the simulations LandAero and No_Aero in the study area during

868 the mixed-phase cloud (left) and deep cloud (right) stages.
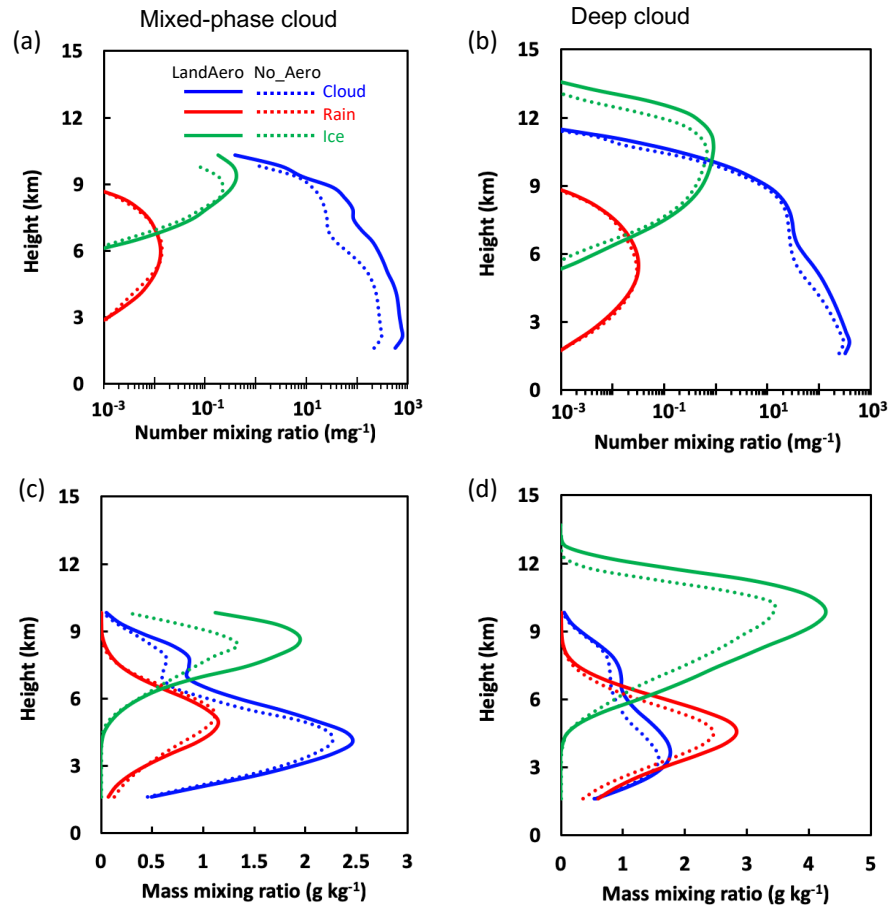
869

870   **Figure 17** Vertical profiles of (a-b) number mixing ratio (mg⁻¹) and (c-d) mass mixing ratio (g

871   kg⁻¹) of cloud droplets (blue), raindrops (red) and ice particles (green) averaged over the top 25

872   percentiles (i.e., 75th to 100th) of the updrafts with a value greater than 2 m s⁻¹ from the

873   simulations LandAero and No_Aero in the study area during the mixed-phase cloud (left) and

874   deep cloud (right) stages.